Scientific Research Publishing

Open Journal of Inorganic Chemistry, 2026, 16(2), 17-54
https://www.scirp.org/journal/ojic
ISSN Online: 2161-7414
ISSN Print: 2161-7406

In Vitro Antischistosomal Potentials of 1-(quinolin-2-yl)-N-(quinolin-8-yl)methanimine, 2-((quinolin-8-ylimino)methyl)quinolin-8-ol and N-(pyridin-2-ylmethyl)-1-(quinolin-2-yl)methanimine] Heteroaryl Schiff Bases and Their Zn(II) Complexes: Synthesis, Characterisation, Density Functional Theory Studies, Molecular Docking and *in Silico* Pharmacokinetics Properties

Celine Kekwi Ngwang[1], Mireille Sylviane Dongmo Nguepi[2], Jean Hubert Nono[3], Marius Belmondo Tincho[2], Mirabel Akongwi[1], Domiriane Ornela Madjougne Foudjo[4], Darline Dize[4], Diana Sandra Wendji Monkam[4], David Woutouoba Ntieche[4], Alvine Kengne[4], Felicite Majoumo-Mbe[1*]

[1]Department of Chemistry, Faculty of Science, University of Buea, Buea, Cameroon
[2]Department of Biochemistry and Molecular Biology, Faculty of Science, University of Buea, Buea, Cameroon
[3]Department of Chemical and Biological Engineering, National Higher Polytechnic Institute, University of Bamenda, Bamenda, Cameroon
[4]Department of Biochemistry, Faculty of Science, University of Yaoundé 1, Yaoundé, Cameroon
Email: *majoumo.felicite@ubuea.cm, *fmajoumo@yahoo.fr

How to cite this paper: Ngwang, C.K., Nguepi, M.S.D., Nono, J.H., Tincho, M.B., Akongwi, M., Foudjo, D.O.M., Dize, D., Monkam, D.S.W., Ntieche, D.W., Kengne, A. and Majoumo-Mbe, F. (2026) *In Vitro* Antischistosomal Potentials of 1-(quinolin-2-yl)-N-(quinolin-8-yl)methanimine, 2-((quinolin-8-ylimino)methyl)quinolin-8-ol and N-(pyridin-2-ylmethyl)-1-(quinolin-2-yl)methanimine] Heteroaryl Schiff Bases and Their Zn(II) Complexes: Synthesis, Characterisation, Density Functional Theory Studies, Molecular Docking and *in Silico* Pharmacokinetics Properties. *Open Journal of Inorganic Chemistry*, **16**, 17-54.
https://doi.org/10.4236/ojic.2026.162002

Abstract

Zn(II) complexes of three heteroaryl Schiff bases **L[1]**, **HL[2]** and **L[3]** of general formula $[ZnL^1Cl_2]\cdot 2H_2O$ (**1**), $[ZnL^2Cl]\cdot H_2O$ (**2**), $[ZnL^3Cl_2]\cdot H_2O$ (**3**) [**L[1]** = 1-(quinolin-2-yl)-*N*-(quinolin-8-yl)methanimine, **HL[2]** = 2-((quinolin-8-ylimino)methyl)quinolin-8-ol, **L[3]** = *N*-(pyridin-2-ylmethyl)-1-(quinolin-2-yl)methanimine] have been synthesised. Based on spectroscopic analyses, five-coordinate geometries were proposed where **L[1]** and **L[3]** coordinated through the azomethine N and the two quinolines N as neutral NNN-donor modes, while **HL[2]** coordinated through the azomethine N, the two quinolines N and the O atom of the OH group as deprotonated with NNNO-donor mode. DFT calculations were used to investigate the electronic properties of the ligands

Received: March 1, 2026
Accepted: April 11, 2026
Published: April 14, 2026

and complexes, and their optimised structures were generated. Complexation and the presence of the OH group enhanced the activity against cercariae of *Schistosoma mansoni* while $\mathbf{L^1}$ with fused benzene backbone and its complex were inactive compared to $\mathbf{L^3}$ with CH_2 backbone from 2-picolylamine derivative. Molecular docking studies revealed that the active compounds displayed higher binding affinity to the active sites of SmCE2a, SER, SmTGR, and SmPNP, with binding energies ranging from −6.1 to −10.1 kcal/mol, indicating that the ligands ($\mathbf{HL^2}$), $\mathbf{L^3}$ and complex (**2**) can be potential inhibitors of the four main target proteins of *S. mansoni*. *In silico* pharmacokinetics properties of $\mathbf{HL^2}$, $\mathbf{L^3}$ and Zn(II) complex (**2**) agree with the four drug likeness rules (Lipinski, Ghose, Veber, and Egan rules) and these derivatives can be considered as potential lead candidates for an antischistosomal therapeutic development. Furthermore, the active ligands and complex showed a good bioavailability score of 0.55.

Keywords

Zn(II) Complexes, Heteroaryl Schiff Bases, DFT Studies, *In Vitro* and *in Silico* Cercaricidal Potential, Pharmacokinetics Prediction

1. Introduction

The chemistry of coordination compounds with heterocyclic ligands containing oxygen and nitrogen as donor atoms has attracted increasing attention because they can exhibit different modes of coordination to a metal centre. Schiff bases are an important class of ligands that have been extensively studied. Aryl Schiff bases are commonly synthesised by the condensation reaction of aromatic aldehydes or ketones with primary amines, resulting in an azomethine moiety with at least one aryl group attached to the carbon or nitrogen atom. The interest in Schiff base ligands is therefore due to their ease of synthesis, selectivity to the central ion [1], synthesis flexibility [2], structural diversity [3], and their broad biological activities [4].

Quinolines are derivatives of pyridine and are found in many biologically active natural and synthetic compounds [5]-[8]. Their Schiff base derivatives have also been reported with various pharmacological activities [9] [10]. Some free Schiff base ligands are known to be active, but literature has shown that the presence of metal in such ligands may increase their activities [11] [12]. Apart from their medicinal properties, Schiff base compounds play an important role as ligands in coordination chemistry. Schiff base ligands that contain multidentate NNN-donor atoms have gained a lot of interest in different fields of coordination chemistry [13]-[16]. Schiff base compounds of 8-hydroxyquinoline are used as chelating agents [17]. Their versatile coordination behaviour is used to prepare various coordination complexes that present interesting properties such as DNA binding ability [18], making them potential targets for anticancer, antimicrobial, antioxidant and

bioimaging agents in living cells [19]-[22]. In general, the imine group, which contains an electrophilic carbon and nucleophilic nitrogen, provides excellent binding opportunities that inhibit targeted diseases [23].

Schistosomiasis, a neglected tropical disease, is the second most endemic parasitic worm disease caused by species of the genus Schistosoma, including *Schistosoma guineensis*, *Schistosoma haematobium*, *Schistosoma intercalatum*, *Schistosoma japonicum*, *Schistosoma mansoni*, and *Schistosoma mekongi* [24]. More than 250 million individuals in tropical and subtropical regions of the world are affected by this neglected tropical disease, especially in deprived communities, which lack access to safe drinking water and adequate sanitation [25]-[27]. High prevalence rates have been recorded in Africa, the Caribbean, Latin America, and Asia, with over 90% of cases reported in Sub-Saharan Africa [28]. Considerable efforts to eradicate schistosomiasis from endemic areas through repeated mass preventive chemotherapy, improvement of water, sanitation, and hygiene, snail control, behavioural changes, and environmental management have not been entirely successful [29]. This is mainly due to the high cost involved in treatment campaigns and the inequity of access to preventive chemotherapy [30] [31].

Praziquantel, which is currently the only drug of choice for treatment, has faced the challenge of reduced drug sensitivity to juvenile parasites and the suspected emergence of drug-resistant strains [32]-[34]. While emphasising the need to eliminate schistosomiasis by 2030, the World Health Organisation (WHO) proposed the development of new intervention tools and alternative drugs to Praziquantel [35] [36]. Proteins have been reported as targets in antischistosomal drug discovery [37]. Recent research reported novel antischistosomal drug targets as inhibitors of SmTGR or SmDHODH (the enzyme dihydroorotate dehydrogenase from *Schistosoma mansoni*) via *in silico* methods [38] [39]. There is an increasing interest in the use of transition metal compounds as new opportunities to fight against drug-resistant pathogens through their antiparasitic activities [40] [41]. The potential of imine-Cu(II) and Zn(II) metal complexes as new lead compounds against adult schistosomes has been reported [42]. The introduction of metal-based compounds in chemical biology has opened the door to developing novel drug treatment options against neglected tropical diseases [43] [44].

We recently reported on some Schiff base metal complexes with biological activity [45]-[51]. In our search for ligational behaviour of small bioactive molecules towards transition metals and the potential bioactivity of their resulting metal complexes against virus responsible for parasitic diseases, we now report on the synthesis, characterisation, Density Functional Theory studies, *in vitro* antischistosomal potential, molecular docking and *in silico* pharmacokinetics predictions of Zn(II) complexes with quinolinyl heteroaryl Schiff bases bearing different backbones derived from quinolin-2-carboxaldehyde, 8-hydroxyquinolin-2-carboxaldehyde with 8-aminoquinoline and 2-picolylamine.

2. Experimental Section

2.1. Materials and Methods

Reagent grade quinolin-2-carboxaldehyde, 8-hydroxyquinolin-2-carboxaldehyde, 8-aminoquinoline, 2-picolylamine and $ZnCl_2$ were purchased from Sigma Aldrich. Ethanol as a solvent was used as purchased. The melting points were determined with a Stuart SMP11 instrument in sealed capillary and are uncorrected. Infrared spectra were obtained (KBr 400 - 4000 cm^{-1}) on an ALPHA FT-IR Spectrometer from Bruker. UV-visible spectra were carried out with a GENESYS 10 S UV-vis spectrophotometer. A Bruker AV 400 MHz Spectrometer was used for the ^{1}H and ^{13}C NMR analyses.

2.2. General Procedure for the Synthesis of L^1 and L^3

The Schiff base ligands L^1 and L^3 used in the synthesis of the Zn(II) complexes were obtained from the condensation reaction of quinolin-2-carboxaldehyde with 8-aminoquinoline and 2-picolylamine, as indicated in Scheme 1. HL^2 was synthesised as reported in the literature [52].

2.2.1. Synthesis of L^1

(1 g, 6.8 mmol) of quinoline-2-carbaldehyde in 50 mL of ethanol was added dropwise with stirring to 8-aminoquinoline (0.97 g, 6.8 mmol) in 50 mL of ethanol in a round-bottom flask. Three drops of glacial acetic acid were added to the mixture. The reaction mixture was then heated to reflux for 4 hours, and the precipitate obtained after cooling overnight was filtered, washed twice with ethanol and dried (1.73 g, 90%). Melting point: 182˚C. FTIR (max/cm^{-1}): 3335 vw, 3048 vw, 1681 vw, 1593.8 (C=N), 1567 w, 1503 s, 1476 w, 1426 w, 1373 m, 1140 w, 820 m, 750 vs, 620 w, 497 m, 423 w. NMR: δH (400 MHz; DMSO): 8.83 (1H, s), 8.72 (1H, dd, J = 4 Hz), 8.50 (1H, dd, J = 8 Hz), 8.29 (1H, dd, J = 8 Hz), 8.16 (1H, d, J= 8 Hz), 8.12 (1H, d, J = 4 Hz), 7.91 (1H, t, J = 8 Hz, J = 12 Hz), 7.84 (1H, d, J =4 Hz), 7.70 (1H, t, J =8 Hz, J = 12 Hz), 7.45 (1H, dd, J = 4 Hz), 7.30 (1H, dd, J = 4 Hz), 7.06 (1H, d, J = 8 Hz), 6.9 (1H, d, J = 4 Hz), 3.41 (H_2O). δC (100 MHz; DMSO): 160.2, 151.0, 147.4, 147.0, 139.0, 138.6, 137.4, 137.2, 136.3, 130.1, 128.9, 128.41, 128.4, 128.3, 127.9, 121.9, 121.3, 114.1, 109.1. UV-vis: λ_{max} (DMSO/nm): 245, 280, 385.

2.2.2. Synthesis of L^3

(1.46 g, 10 mmol) of quinoline-2-carbaldehyde in 50 mL of ethanol was added dropwise with stirring to 2-picolylamine (1 mL, 10 mmol) in 50 mL of ethanol in a round-bottom flask. Three drops of glacial acetic acid were added to the mixture. The reaction mixture was then heated to reflux for 4 hours, and the precipitate obtained after cooling overnight was filtered, washed twice with ethanol and dried (1.65 g, 67%). Melting point: 262˚C. FTIR (max/cm^{-1}): 3300 br, 3054 w, 2926 w, 2855 w, 1673 w, 1588 s (C=N), 1566 w, 1496 w, 1461 s, 1425 s, 1144 m, 1110 w, 1090 w, 1044 w, 1014 w, 995 m, 836 m, 744 vs, 694 w, 617 m, 476 m, 425 w, 401 m. NMR: δH (400 MHz; DMSO): 8.56 (1H, t, J = 8 Hz, J = 12 Hz), 8.35 (1H, d, J = 8 Hz), 8.30 (1H, s), 8.07 (1H, d, J = 8 Hz), 7.95 (1H, t, J= 8 Hz, J = 12 Hz), 7.87

(1H, d, J = 8 Hz), 7.72 (1H, d, J = 8 Hz), 7.49 (1H, t, J = 4 Hz, J = 12 Hz), 7.39 (1H, t, J = 8 Hz, J = 12 Hz), 7.28 (1H, t, J = 4 Hz, J = 8 Hz), 7.09 (1H, t, J = 4 Hz, J = 8 Hz), 6.83 (1H, d, J = 4 Hz), 4.72 (2H, d, J= 4 Hz), 3.45 (H_2O). δC (100 MHz; DMSO): 166.7, 162.2, 156.8, 150.9, 149.0, 137.3, 136.9, 130.9, 128.7, 128.6, 128.5, 126.0, 123.4, 122.4, 119.1, 62.0. UV-vis: λ_{max} (DMSO/nm): 250, 300, 390.

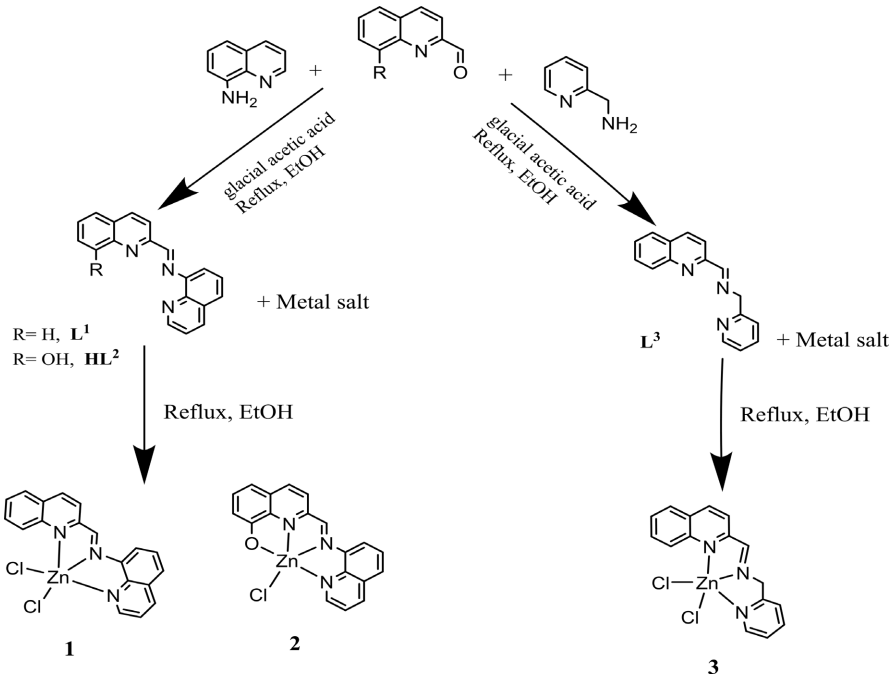

Scheme 1. Synthesis of **L¹**, **HL²**, **L³** ligand and their **1**, **2**, and **3** Zn(II) complexes.

2.3. General Procedure for the Synthesis of Zn(II) Complexes

2.3.1. Synthesis of $[ZnL^1Cl_2]\cdot 2H_2O$ (1)

A 20 mL ethanol solution of $ZnCl_2$ (0.136 g, 1 mmol) was added dropwise to a 30 mL hot ethanol solution of L^1 (0.283 g, 1 mmol) while stirring. The resulting mixture was refluxed for 5 hours, and the resulting precipitate obtained on cooling overnight was filtered, washed with ethanol and dried (0.34 g, 83%). Melting point: >285˚C. FTIR (max/cm^{-1}): 3393 w, 3059 w, 1594.3 s (C=N), 1505 s, 1450 w, 1429 m, 1379 m, 1343 w, 1218 w, 1146 w, 1071 w, 833 s, 759 vs, 620 w, 477 m, 449 w, 417 w. NMR: δH (400 MHz; DMSO): 9.17(1H, dd, J = 4 Hz), 8.91 (1H, s), 8.73 (1H, d, J = 8 Hz), 8.53 (1H, t, J = 8 Hz, J = 4 Hz), 8.17 (1H, t, J= 4 Hz, J = 8 Hz), 7.98 (1H, d, J = 8 Hz), 7.89 (1H, dd, J= 4 Hz), 7.80 (1H, t, J =4 Hz, J = 8 Hz), 7.73 (1H, dd, J = 4 Hz, J = 8 Hz), 7.66 (1H, d, J = 4 Hz), 7.30 (1H, t,, J = 4 Hz, J = 8 Hz), 7.18 (1H, brs), 7.02 (1H, d, J = 8 Hz), 3.39 (H_2O). ^{13}C NMR was not obtained due to low resolution. UV-vis: λ_{max} (DMSO/nm): 255, 283, 585. Molar Conductivity: 15.1 $S\cdot cm^2\cdot mol^{-1}$.

2.3.2. Synthesis of $[ZnL^2Cl]\cdot H_2O$ (2)

A 20 mL hot ethanol solution of $ZnCl_2$ (0.136 g, 1 mmol) was added dropwise to a 30 mL hot ethanol solution of HL^2 (0.299 g, 1 mmol) while stirring. The resulting

mixture was refluxed for 5 hours, and the precipitate obtained on cooling overnight was filtered, washed with ethanol and dried (0.32 g, 81%). Melting point: >339˚C. FTIR (max/cm^{-1}): 3336 br, 3055 w, 1597 w (C=N), 1573 s, 1505 s, 1435 m, 1376 m, 1330 m, 1241 m, 1196 w, 1110 m, 1087 m, 820 s, 787 s, 750 vs, 721 w, 539 w, 498 w, 463 m, 434 w, 419 m. NMR: δH (400 MHz; DMSO): 8.84 (1H, s), 8.72 (1H, dd, J = 4 Hz), 8.48 (1H, d, J = 4 Hz), 8.17 (1H, dd, J= 8 Hz), 7.86 (1H d, J = 4 Hz), 7.72 (1H, dd, J =4 Hz, J = 8 Hz), 7.54 (1H, t, J = 4 Hz, J = 8 Hz), 7.45 (1H, dd, J = 4 Hz), 7.28 (1H, dd, J = 4 Hz, J = 8 Hz), 7.05 (1H, d, J = 4 Hz), 6.88 (1H, d, J = 4 Hz), 6.78 (1H, d, J = 8 Hz), 3.38 (H_2O). δC (100 MHz; DMSO): 193.8, 156.5, 154.3, 151.8, 147.7, 147.4, 145.7, 137.9, 136.3, 134.8, 129.0, 128.1, 124.5, 121.9, 121.4, 118.3, 114.2, 109.1, 106.4. UV-vis: λ_{max} (DMSO/nm): 275, 330, 590. Molar Conductivity: 35.9 $S{\cdot}cm^2{\cdot}mol^{-1}$.

2.3.3. Synthesis of $[ZnL^3Cl_2]{\cdot}H_2O$ (3)

A 20 mL hot ethanol solution of (0.136 g, 1 mmol) $ZnCl_2$ was added dropwise to a 30 mL hot ethanol solution of L^3 (0.247 g, 1 mmol). The resulting mixture was refluxed for 5 hours and the precipitate obtained after cooling overnight was filtered, washed with ethanol and dried (0.28 g, 73%). Melting point: 281˚C. FTIR (max/cm^{-1}): 3392 br, 3075 w, 1596 s (C=N), 1568 w, 1509 m, 1477 m, 1434 m, 1378 w, 1343 w, 1294 m, 1216 m, 1148 w, 1051 w, 1016 w, 832 m, 756 vs, 637 w, 483 w, 410 w. NMR: δH (400 MHz, DMSO): 9.02 (1 H, s), 8.78 (1H, dd, J = 8 Hz) 8.56 (1H, d, J = 4 Hz), 8.45 (1H, t, J = 4 Hz, J = 8 Hz), 8.33 (1H, t, J = 4 Hz, J = 8 Hz), 8.17 (1H, t, J = 4 Hz, J = 8 Hz), 8.07 (1H, t, J = 4 Hz, J = 8 Hz), 7.96 (1H, dd, J =4 Hz), 7.79 (1H, dd, J =4 Hz, J = 8 Hz), 7.72 (1H, dd, J = 4 Hz), 7.61 (1H, dd, J = 4 Hz), 4.81 (2H, s), 3.44 (H_2O). δC (100 MHz, DMSO): 166.5, 164.7, 158.5, 156.9, 155.6, 149.4, 147.5, 146.5, 144.2, 141.3, 138.2, 137.2, 130.9, 129.8, 128.5, 124.2, 121.7, 60.4. UV-vis: λ_{max} (DMSO/nm): 265, 330, 395. Molar conductivity: 17.8 $S{\cdot}cm^2{\cdot}mol^{-1}$.

2.4. Biological Methodology

2.4.1. Cercaricidal Activity

The cercaricidal activity was assessed according to the protocol described by Dongmo Nguepi *et al.* [53] with some modifications. Briefly, stock solutions of compounds dissolved in DMSO (20 mg/mL) were diluted using distilled water to obtain a concentration of 2 mg/mL and to bring down the concentration of DMSO to at most 1% in the test plate. Cercariae suspensions corresponding to 20 cercariae per well were inoculated in the wells of a 96-well plate, and solution was added to make final concentrations of 200, 40, 8, 1.6, 0.32, and 0.064 µg/mL. The independent biological repeats were done in duplicates and incubated for 3 hours. Triplicates were used, and controls: Niclosamide 1% as a positive control and distilled water as a negative control. The cercaricidal activity of the compounds was read microscopically from the mortality of cercariae.

2.4.2. Cytotoxicity Test

The biosafety assessment was conducted using African green monkey Vero cells

(ATCC-CRL-1586). The assay was performed according to the protocol described by Balbaied and Moore (2020) [54] with some slight modifications. Briefly, 100 µL of cell suspension was distributed in each well of a 96-well plate at a charge of 1×10^4 cells/well and followed by an incubation of the plate at 37˚C, 5% CO_2 for 18 hours for cell seeding. After this, the culture medium was gently removed with the aid of a pipette and replaced by 90 µL of fresh DMEM medium pre-heated at 37˚C and 10 µL of each concentration for all the samples was added to the plate. The wells with only cells and culture medium constituted the negative control while those containing cells and culture medium supplemented with 10 µL of podophyllotoxin at 50 µM represented the positive control and the plate was incubated at 37˚C, 5% CO_2 for 48 hours. After the treatment of cells with the different compounds, 10 µL of resazurin solution (0.15 mg/mL) was added and the fluorescence signal was allowed to develop for 3 - 4 hours, after which the optical density was read using an infinite microplate reader (Tecan) at a wavelength of excitation and emission of 530 and 590 nm, respectively. The selectivity index (SI) is defined as the ratio of the Vero cells toxicity to the cercaricidal activity and was determined by dividing the CC_{50} values by the LC_{50} values of the active compounds. It reflects the effectiveness against target parasites while minimising toxicity to host cells.

2.5. Methodology for DFT Analysis

Theoretical analysis of structural and electronic properties of the synthesised ligands (L^1, HL^2 and L^3) and their Zn(II) complexes was carried out using the hybrid meta exchange correlational functional m06 [55] associated with 6 - 31++g (d, p) basis set [56]. This basis set contains polarised functions that improve the flexibility of the basis set and diffuse functions, which are appropriate to handle anions and high electronegative elements such as chlorine. These functions are essential to accurately determine the geometry, the energy and non-covalent interactions of the investigated system. Although the m06 functional already includes long-range correction, and additional dispersion correction was included through Grimme's D3 model [57] to improve on the optimised geometry. All calculations were carried out in the vacuum with the aid of Gaussian 16, Revision C.01 package [58] while GaussView 6.0.16 [59] visualisation program was used to build the structures and to analyse the obtained results. The starting molecular geometries for the optimisation process were proposed based on information obtained from spectroscopic and physicochemical characterisation of the compounds. The molecules were optimised using *tight criteria* and the values of the frequencies of the normal modes of vibration of the optimised structures were determined at the same levels of theory to ensure no imaginary frequency. The studied molecules were considered neutral and were optimized following the restricted scheme as they are all closed shells. Bader's quantum theory of atom in molecules [60], reduced density gradient method [61] and Wiberg bond index implemented in Multiwfn 3.8 were used to characterise metal-ligand interactions. The distribution of

HOMO and LUMO and the molecular electrostatic potential (MEP) map [62] [63] at the surface of optimised molecules were used to investigate their electrophilic and nucleophilic regions. HOMO-LUMO gap ($\Delta E_g = E_{LUMO} - E_{HOMO}$), chemical potential ($\mu = \frac{E_{LUMO} + E_{HOMO}}{2}$), electronegativity ($\chi = -\mu$), ionisation potential ($IP = -E_{HOMO}$), electron affinity ($EA = -E_{LUMO}$), chemical hardness ($\eta = \frac{E_{LUMO} - E_{HOMO}}{2}$), chemical softness ($S = \frac{1}{\eta}$), electrophilic index ($\omega = \frac{\mu^2}{2\eta}$) and the maximum electron density ($\Delta N_{max} = -\frac{\mu}{\eta}$) were used to predict the interaction of the study's compounds with their environment [64]-[66].

2.6. Docking Computing Details

Docking experiments were conducted to assess the binding affinity between the active compounds and four important protein drug targets of schistosomes using the command prompt of the web server CB-DOCK 2 (https://cadd.labshare.cn/cb-dock2/php/blinddock.php). CB-Dock is a protein-ligand blind computational biology docking server which employs a protein-surface-curvature-based cavity detection approach to identify cavities or binding sites on the surface of given proteins, to guide the molecular docking with Auto Dock Vina [67].

The 3D structure of the two different proteins of *S. mansoni* Sm thioredoxin glutathione reductase SmTGR (PDB code: 2X8H) and Sm purine nucleoside phosphorylase SmPNP (PDB code: 3FAZ) were received from the Protein Data Bank (PDB) (https://www.rcsb.org/); while Schistosoma epidermal growth factor receptor SER (Uniprotkb code: Q26569) and *Schistosoma mansoni* cercarial elastase 2a SmCE2a (Uniprotkb code: Q8MUV8) protein sequences were extracted from Uniprotkb, and their 3D structures were determined using the I-TASSER online server (https://zhanggroup.org/I-TASSER/). I-TASSER server implements the I-TASSER-based algorithms for protein structure and function predictions. It detects structure templates from the Protein Data Bank by a technique called fold recognition. To evaluate the docking of each Schistosoma protein and the different compounds with the CB-Dock server, the PDB format of the protein and the PDB file of the query compound were uploaded into the CB-Dock server and the "Auto-blind docking" parameter was selected. CB-Dock2 improves protein-ligand blind docking by integrating cavity detection, docking and homologous template fitting. This server utilises fitdock doc-king method and AutoDock Vina for template-independent blind docking and the results are given as vina score (ranges from −3.8 to −18) [67]. The visualisation and analysis present the results, which can be visualised and analysed by interactive NGL Viewers for 3D structures and 2D sequences, together with abundant information about binding sites, template structures, binding scores, contact residues, docking centre, and cavity volume.

3. Results and Discussion

3.1. Spectroscopic Characterisation of the Schiff Base Ligands and Their Zinc(II) Complexes

The IR spectra provide very interesting information about the nature of functional groups present in the ligand, which can be attached to the central metal atom. Selected IR frequencies of ligands and complexes are presented in **Table 1**. **Figure S1** (see supplementary images) shows the IR spectra of ligands and Zinc(II) complexes. The spectra of the ligands showed characteristic prominent bands at 1593.8, 1596 [52] and 1588 cm^{-1} due to the azomethine band (C=N) respectively for L^1, HL^2 and L^3 and the O-H stretching and bending vibrations in HL^2 were assigned to bands at 3368 and 1235 cm^{-1} respectively. C=N imine vibrations in some reported quinolines Schiff base derivatives were assigned in the range of 1550 - 1650 cm^{-1} [20], 1594 cm^{-1} [68] and the aromatic O-H stretching and bending vibrations were reported in the range 3367 - 3371 cm^{-1} [69], 3377 cm^{-1} [52] and 1240 cm^{-1} [52], 1282 cm^{-1} [70] or 1300 cm^{-1} [71] respectively. Upon coordination, the imine bonds of the Zn(II) complexes 1, 2 and 3 shifted to the higher vibrations of 1594.3, 1597 and 1596 cm^{-1} respectively, indicating the participation of that group in coordination. In the spectra of each ligand, two mid-intensity bands appear at (1140, 750), (1085, 747) and (1144, 744) cm^{-1}, which are assigned to the pyridine or quinoline ring bending and outside the plan deformation respectively [72]. These bands are shifted to the higher values by 2 - 12 cm^{-1} in the spectra of the Zn(II) complexes, indicating that the quinoline and pyridine nitrogen are involved in coordination with the metal ion. Displacements to higher values of 1241 cm^{-1} in the zinc complex of HL^2 also appear for the C-O bending of the hydroxyl group, indicating coordination of the oxygen to the metal through deprotonation [70]. All the IR data support the idea that in (1) and (3) complexes, the ligands L^1 and L^3 works as tridentate NNN, while in (2), HL^2 acts as a tetradentate NNNO, being coordinated through the azomethine nitrogen, the pyridine and quinoline nitrogen and the hydroxyl oxygen. New weak intensities, non-ligand bands are observed in the region 417, 410 cm^{-1} and 419, 498 cm^{-1} in (1), (3) and (2) respectively, indicating the formation of M-N and M-O bonds [70] [73].

Table 1. Selected IR frequencies (cm^{-1}) of ligands and Zn(II) complexes.

Compounds	υ (O-H)	υ (C=N)	υ (C-O)	υ (Ar. bending)	υ (Ar. out of plane deformation)	υ (M-O)	υ (M-N)
L^1	3335	1593.8	-	1140	750	-	-
HL^2	3368	1596	1235	1085	746	-	-
L^3	3300	1588	-	1144	744	-	-
1	3393	1594.3	-	1146	759	-	417
2	3336	1597	1241	1087	750	498	419
3	3392	1596	-	1148	756	-	410

The ^{1}H NMR spectra of the ligands and their Zn(II) complexes were determined. In the free ligand, the distinct peak of the azomethine HC=N was observed at 8.83, 8.80 [52] and 8.30 ppm, for L^1, HL^2 and L^3 respectively. A significant downfield shift of this proton to 8.90, 8.84 and 9.00 ppm was detected in complexes (1), (2) and (3). These results indicated the coordination of the nitrogen of the azomethine to the metal ion. The chemical shift at 10.23 ppm, corresponding to the proton of the hydroxyl group of HL^2, disappeared upon complex formation. The deprotonation of this proton leads to the coordination of the oxygen atom toward the Zn(II) ion in complex 2. Moreover, chemical shifts in the range of 6.76 - 8.72 (6.93 - 8.25 ppm) [52] and 6.83 - 8.56 ppm assigned to protons of quinoline rings of ligands L^1, HL^2 and quinoline and pyridine rings of L^3, also presented significant shifts in the range 6.78 - 9.17 ppm and 7.61 - 8.78 ppm upon the formation of complexes 1, 2 and 3 respectively. This result could affirm the binding of the nitrogen donors of this heterocyclic aromatic and pyridine rings to the zinc metal ion.

Electronic spectral analysis of ligands exhibited three major absorption bands in the range 245 - 250 nm, 280 - 300 nm and 380 - 390 nm, that may be attributed to the π-π^* transitions of the aromatic system, π-π^* transitions of the azomethine and n-π^* transition due to the lone pair electrons of the azomethine N [68]. Electronic spectra of Zn(II) complexes showed transition bands in the ranges of 255 - 275 nm, 283 - 330 nm, confirming their intra-ligand charge transfer transitions. Additional new bands at 585, 590 and 395 nm in complexes (1), (2) and (3) respectively were attributed to metal-ligand charge transfer (CT) [69]. The observed shift associated with the decrease in intensity of the absorption bands may be attributed to the coordination of the ligand heteroatoms to the metal centre. **Figure S2** (see supplementary images) shows the electronic spectra of ligands and Zn(II) complexes. The lower values of 15.1, 35.9 and 17.8 $S{\cdot}cm^2{\cdot}mol^{-1}$ of molar conductivity in DMSO for (1), (2) and (3) respectively, indicated that the complexes are non-electrolytes in solution [74]. Based on spectroscopic analyses, L^1 and L^3 ligands can be considered as neutral tridentate with *NNN*-donor site in their Zn(II) complexes (1) and (3), giving the proposed five coordinate geometries. On the other hand, HL^2 ligand in its Zn(II) complex (3) shows a monobasic tetradentate *NNNO*-donor site, giving also a proposed five coordinate geometry.

3.2. Thermogravimetric Analyses of Zn(II) Metal Complexes

The Zn(II) complex (1) was thermally decomposed in two steps. The first decomposition step gave an observed mass loss of 7.98% (calc. 7.94%), which occurred within the range from 25 to 180˚C. This step might be attributed to the loss of two molecules of crystallization water. The second decomposition step occurred over the range 200˚C - 560˚C with two DTA exothermic peaks in the 410˚C - 460˚C and 470˚C - 510˚C, in which the complex lost the organic fragments, Cl_2 and NO_2 with an observed mass loss of 85.06% (calc. 85.23%). The horizontal line in the TGA beyond 590˚C indicated the formation of ZnO residue as the final product

of decomposition.

The Zn(II) complexes (2) and (3) gave a decomposition pattern of three stages. The first step of decomposition between 25˚C - 140˚C and {25˚C - 180˚C} with weight loss observed of 3.65% (calc. 4.34%) and {4.31% (calc. 4.51%)} respectively, can be attributed to the loss of one water molecule of hydration. The second step of decomposition was between 140˚C - 290˚C and {200˚C - 470˚C} with an observed weight loss of 10.09% (calc. 10.62%) and {20.36% (calc. 20.42%} respectively, which can be attributed to the loss of one molecule of CO_2 and {1/2 chlorine and NO_2}. The third step of decomposition between 300˚C - 600˚C and {480˚C - 600˚C,} with an observed weight of 82.77% (calc. 82.00%) with two exothermic DTA peaks in the range 460˚C - 520 C and 570˚C - 600˚C and {64.54% (calc. 64.31%) with an exothermic DTA in the rage of 580˚C - 680˚C}, that may correspond to the loss of NO, Cl_2 and two $C_{10}H_7N$ molecules and {the loss of chlorine and complete decomposition of the ligand} respectively. No further mass loss was observed beyond 600˚C and 700˚C respectively in 2 and 3 where the presence of a horizontal line indicated that zinc oxide may be the residual final product. The TGA analyses generally show the presence of water molecules of crystallisation and confirm the proposed general formula of the Zn complexes. **Figure S3** (see supplementary images) shows the TGA graph of Zn(II) complexes.

3.3. Biological Evaluation

3.3.1. Cercaricidal Activity

The anticercarial activity was examined for the ligands and their metal complexes against the *S. mansoni* cercariae obtained from *Biomphalaria pfeifferi* snails. The lethal concentration LC_{50} and the median cytotoxic concentration CC_{50} of the active compounds are presented in **Table 2**. The results of anticercarial activity show that the ligands HL^2 and L^3 show a very good to good activity with an LC_{50} of 1.23 and 19.92 µg/ml [75].

Table 2. Median lethal concentrations (LC_{50}), median cytotoxic concentration (CC_{50}) and selectivity index (SI).

Compounds	LC_{50} µg/mL (mean ± SD)	CC_{50} µg/mL (mean ± SD)	SI
L^1	Not active	ND	-
HL^2	1.23 ± 0.08	65.32 ± 1.29	53.10
L^3	19.92 ± 1.77	>100	>5.02
1	Not active	ND	-
2	1.14 ± 0.14	51.11 ± 4.61	44.83
3	ND	ND	-
Niclosamide	<0.5	ND	-

The significant difference in potency between the two ligands suggests that specific structural features or mechanisms of action may be responsible for the observed

cercaricidal activity. This difference may be due to the presence of one hydroxyl group in HL^2, which increases its lipophilicity as it has been reported that large heteroaromatic moieties are generally more effective against the larval stage of *S. mansoni* [76]. Upon complexation, 2 with LC_{50} of 1.14 μg/ml shows increasing activity compared to the free ligand (1.23 μg/ml). Among the tested compounds, HL^2 and its Zn(II) complex 2 show higher activity and can be considered as lead compound for antischistosomal activity. L^1 and its complex, even at higher concentrations, were inactive compared to L^3 with 2-picolylamine derivative. This increase in activity with the CH backbone was also observed in the catalytic activity of Ni(II) complex compared to the phenyl backbone [16].

3.3.2. Cytotoxicity Activity

To evaluate the safety profile of the compounds, the cytotoxic assay of the active compound was performed on Vero cells. According to the US National Cancer Institute guidelines, a median CC_{50} > 30 μg/mL is non-cytotoxic and <30 μg/mL is cytotoxic [77]. Compounds are generally considered to have significant cytotoxic potential when the CC_{50} is ≤30 μg/ml [78]. Since the observed CC_{50} exceeds this threshold, the compounds do not meet the NCI's criterion for strong cytotoxic activity. Also, it can be noticed that the complexation with Zn(II) metal decreases the cytotoxicity CC_{50} of the ligand. The selectivity index of HL^2 of 53.10 was higher than that of complex 2 of 44.83, but both are in the similar range of non-cytotoxicity, indicating that HL^2 and its Zn(II) complex 2 have the best SI among the tested compounds and can be potential candidates for therapeutic development against schistosomiasis.

3.4. DFT Studies

3.4.1. Geometry Optimisation

The optimised geometry of the ligands and their coordination compounds at 6 - 31++g (d, p)/m06-D3 level of theory (**Figure 1**) shows that L^1 and L^3 act as a tridentate *NNN*-donor ligand and HL^2 acts as a tetradentate *NNNO*-donor ligand. In all these complexes, Zn^{2+} ions are penta-coordinated, and it is found in trigonal-bipyramidal geometry for 1 and 3 and in square-pyramidal geometry in 2. These results are confirmed by the molecular graphs of the studied compounds (**Figure 1**) derived from Bader's quantum theory of atom in molecules [60], which show the presence of bond critical point (yellow balls) and bond path (orange lines) between nitrogen/oxygen/chlorine atoms and Zn(II) ions. The properties of the electron density function at the BCP of various coordination bonds were used to characterise metal-ligand bonds in the study compounds. Therefore, the electronic density, ($\rho(r)$), the Laplacian of the electronic density function, ($\nabla^2\rho(r)$), the total electronic density, ($H(r)$) and the negative ratio of $G(r)$ and $V(r)$) were calculated at the various BCPs and the results are reported in supplementary **Table S1**. It was found that for all coordination bonds in these compounds: $0.039076 \le \rho(r) \le 0.082841$, $\nabla^2\rho(r) > 0$, $H(r) < 0$, $0.5 < -\frac{G(r)}{V(r)} < 1$ which

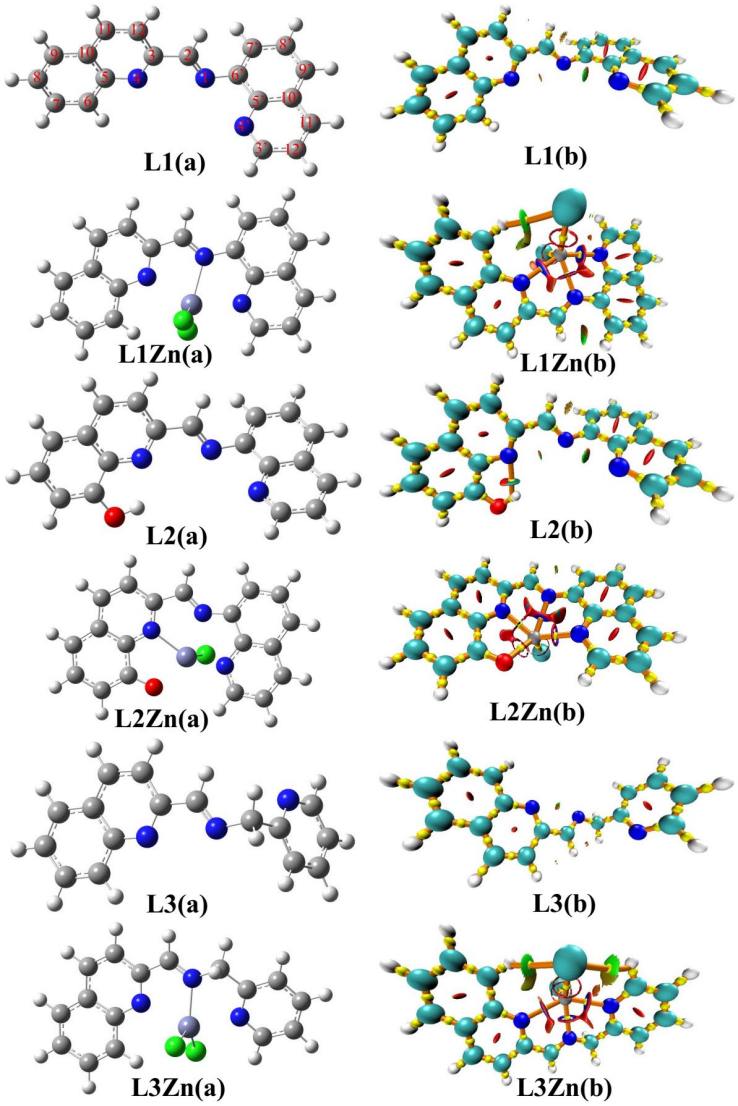

Figure 1. Optimised geometries of ligands and Zn(II) complexes (a) and their molecular graphs associated to their NCIs iso-surface (b) (L2 = HL2; L1Zn = 1; L2Zn = 2; L3Zn = 3).

are characteristic of intermediate interactions that is partial covalent bonds. The 3D isosurface of non-covalent interactions of the various compounds derived from the reduced density gradient method combination [79], combined with molecular graphs (**Figure 1**), reveals the existence of weak van der Waals interactions (green surfaces) such as H---H in all the investigated compounds and C-H---Cl in all the Zn(II) complexes. Strong O-H---N hydrogen bond is found in HL^2 while steric repulsive interactions are observed at the centre of the various rings present in the ligands as well as in the complexes.

The values of selected bond length and bond angles of the optimised geometry of ligands and Zn(II) complexes are reported in supplementary **Table S2**. From these values, 2 has the shortest N4-Zn^{2+}, N4'-Zn^{2+} and Cl-Zn^{2+} bonds, whereas it has the longest values of the N1-Zn^{2+} bond. This result is attributed to the fact that HL^2 is deprotonated in 2, which enhances the ligand-metal charge transfer in the

concerned complex. The formation of 2 is governed by the formation of the O-Zn^{2+} bond as the O atom is negatively charged; therefore, it is formed in such a way to maximise the interactions between O and N4 atoms and the Zn(II) ion. This explains the following decreasing order of the coordination bonds in 2: N1-Zn > N4'-Zn > N4-Zn > O-Zn. The results of the bond length also show that, apart from the N1-Zn bond, N-Zn bonds are shorter in 1 compared to 3 and Cl-Zn bonds are similar in the two complexes. The trigonal-bipyramidal and square-pyramidal geometries around the Zn(II) ions are all distorted due to the constraint of the formation of the five members' ring.

From the data presented in **Table S2**, it can also be concluded that, although the various rings are planar, the three ligands are not planar, neither in the isolated form nor in the complexes. The calculated values of bonds length and angles within the coordination sphere were closer to experimental and theoretical results of coordination compounds with a similar environment found in literature [80]. The strength of the various metal-ligand bonds was investigated using the Wiberg bond index (WBI) calculated as implemented in the Multiwfn 3.8 software. The variation of the Wiberg bond index of the coordination bonds of the different complexes is shown in supplementary **Table S1**. From these values, Zn-Cl bonds have the highest value of WBI (which increases in the order $L^1Zn < L^3Zn < L^2Zn$), followed by Zn-O bonds. In general, L^1Zn has the lowest values of WBI of Zn-X (with X = N, O and Cl) while L^2Zn has the highest values. These results suggest that metal-ligand bonds are stronger in L2Zn, followed by L^3Zn; the interaction between L^1 and Zn is less intense due to the small ligand-metal charge transfer in this complex. This observation may explain the fact that Zn(II) ion has the highest atomic charge (1.333) in L^1Zn compared to 1.057 and 0.851 in L^2Zn and L^3Zn respectively. The analysis of the figure suggests that the strength of Zn-N increases in the order Zn-N1 < Zn-N4 < Zn-N4' in L^1Zn and L^2Zn and Zn-N4 < Zn-N4' < Zn-N1 in L^3Zn.

3.4.2. Frontier Molecular Orbitals (FMOs)

Frontier molecular orbitals in general and particularly the highest occupied molecular orbital (HOMO) and lowest unoccupied molecular orbital (LUMO) play a key role during chemical reactivity and their properties are usually used to predict the chemical reactivity of molecules and to some extent their biological activities. The distribution of HOMO and LUMO on the molecule is related to the regions of the molecule with electron excess and electron deficiency respectively. The energy of the HOMO and LUMO is generally associated with the ability of the molecule to donate and to accept electrons respectively, whereas the energy difference between these orbitals mainly characterises the easiest with which a molecule interacts with its environment. The distribution of the FMOs of both ligands and their Zn(II) coordination compounds is presented in **Figure 2**. It is observed that both HOMO and LUMO of the L^3 ligand are concentrated on the surface of the aldehyde rings, while for L^1, the LUMO is concentrated on the aldehyde ring and the HOMO on the aminoquinoline ring. For HL^2, the LUMO is concentrated on the aldehyde ring and the HOMO on the surface of the two quinoline rings. For

L^1Zn and L^3Zn, the HOMO is totally carried by the Cl atoms, while in L^2Zn, it is carried by the quinoline ring linked to the deprotonated O atom. The LUMO of the three Zn(II) complexes is distributed on the overall surface of the ligands.

The values of HOMO-LUMO energy gap (ΔE_g) of the investigated compounds are also reported in Figure 2. From these values, HL^2 is the most reactive of the three ligands, while L^3 is the least reactive. Therefore, the addition of the OH group in L^1 has a destabilising effect although it favours the formation of a strong hydrogen bond with the nitrogen atom of the same ring. The high instability of L^1 and HL^2 compared to L^3 is attributed to electrostatic repulsion between the electron lone pairs of the various heterogeneous atoms, which are found in the same region of space in those ligands. For L^3, thus to the tetrahedral geometry of Csp^3, only two (2) of these nitrogen atoms are found in the same region (N1-C6'-C5'-N4' = 90˚). The resulting Zn(II) complexes are less stable than their isolated ligands. However, their stability follows the same order of isolated ligands, *i.e.*, L^2-Zn is the least reactive coordination compound, followed by L^1-Zn.

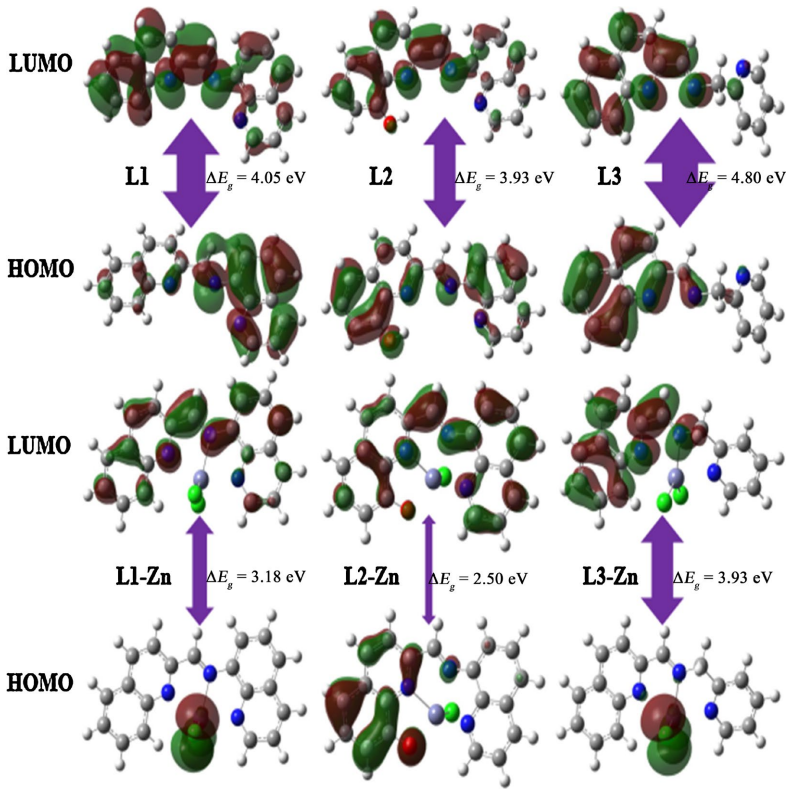

Figure 2. HOMO and LUMO distribution of ligands and their Zn(II) complexes.

Global reactive descriptors of the studied compounds were determined using the conceptual DFT based on the Kopman's approximation. Table 3 summarised the values of the ionisation potential (*IP*), electron affinity (*EA*), electronegativity (χ), chemical potential (μ), hardness (η), softness (S) and electrophilicity (ω) index and the maximum number of electrons (ΔN_{max}) that each compound can acquire. The calculated values of the chemical potential and the hardness show that complexes

are less stable than their corresponding isolated ligands, as predicted by the HOMO-LUMO energy gap.

The hardness of these compounds increases as follows: $L^2Zn < L^1Zn < L^3Zn < HL^2 < L^1 < L^3$. The electrophilicity index reveals that complexes have higher electrophilic power compared to ligand and acquire more electron density than isolated ligands. Electrophilic power and the maximum number of electrons each of these compounds can acquire increase according to the following order: $L^3 < L^1 < HL^2 < L^3Zn < L^1Zn < L^2Zn$. For the investigated compounds, the reactivity varies in the same order as the electrophilic power. The electron affinity of the studied compounds increases in the same order as the electrophilic index, except that the position of L^1Zn and L^2Zn is interchanged. The ionisation potential increases as follows in the series: $L^2Zn < L^1 = HL^2 < L^1Zn < L^3Zn < L^3$. From these results, L^2Zn is the softest of the studied molecules; it has the lowest value of IP and the highest value of ω, while L^3 is the hardest compound with the highest IP and lowest ω.

Table 3. Values (in eV) of some descriptors of the global reactivity of the studied compounds.

Compounds	*IP*	*EA*	μ	χ	η	*S*	ω	ΔN_{max}
L^1	6.21	2.16	−4.18	4.18	2.02	0.49	4.32	2.07
HL^2	6.21	2.28	−4.24	4.24	1.97	0.51	4.57	2.16
L^3	6.77	1.97	−4.37	4.37	2.4	0.42	3.98	1.82
L1Zn	6.67	3.18	−4.93	4.93	1.74	0.57	6.97	2.83
L2Zn	5.48	2.98	−4.23	4.23	1.25	0.8	7.16	3.39
L3Zn	6.73	2.8	−4.76	4.76	1.96	0.51	5.78	2.43

3.4.3. Molecular Electrostatic Potential (MEP)

The molecular electrostatic potential map of the studied compounds was used to determine their regions with positive and negative electrostatic potential and therefore predict their interactions with other molecules during chemical reactions and biological activity [81]. The MEP map of the studied compounds is presented in **Figure 3**.

It is observed that for all the investigated compounds, nitrogen, oxygen and chlorine atoms carry the negative electrostatic potential while C and H carry the positive electrostatic potential. N1 atom carries the most negative electronegative potential of the three ligands, followed by N4' in L1 and L2. In L3, N4 is more nucleophilic than N4', probably due to electron delocalisation. The results suggest that the reaction between the three ligands and the Zn^{2+} starts with the interaction between N1 and Zn^{2+}, which clearly explains why N1-Zn^{2+} is the shortest bond, followed by N4'-Zn^{2+} in L1Zn and L3Zn. The trend of coordination bond length in the L2Zn is attributed to the fact that HL^2 is deprotonated. In the complexes, the highly negative potential is carried by Cl atoms. However, it is important to note that the blue colour of the surface around H atoms is more intense in the complexes

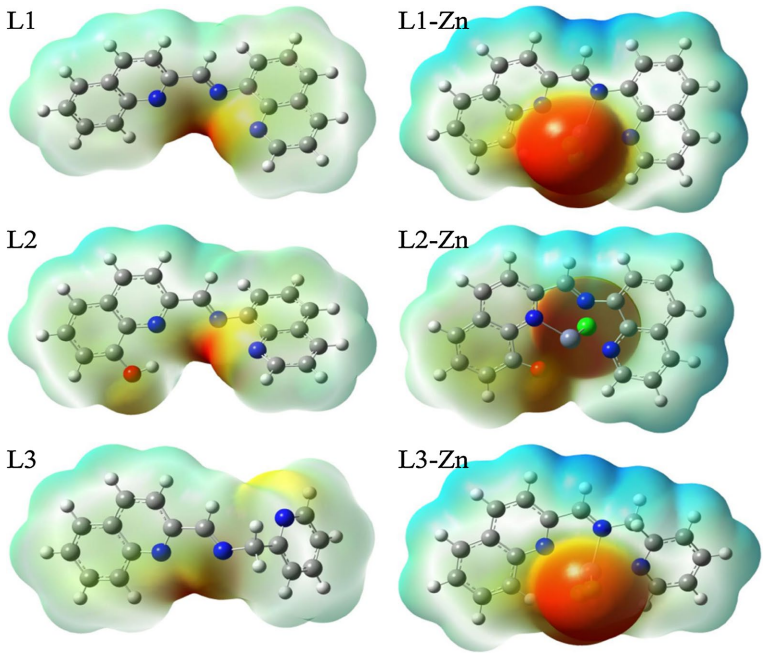

Figure 3. MEP of ligands and their Zn(II) complexes.

than in the isolated ligand, which suggests that the electrophilicity of the concerned increases upon chelation. The H atom of the imine function is the most acidic proton of all the studied compounds, and it is more acidic in the complexes due to the Ligand-metal charge transfer that occurs during the chelation process.

3.5. Molecular Docking Simulations

To assess the molecular interactions and the binding affinity of the active compounds with 4 important target proteins of schistosomes parasites: *Schistosoma mansoni* Cercarial Elastase 2a (SmCE2a), Schistosoma Epidermal growth factor Receptor (SER), *Schistosoma mansoni* Thioredoxin Glutathione Reductase (SmTGR), *Schistosoma mansoni* Purine Nucleoside Phosphorylase (SmPNP), molecular docking predictions were performed, and the results are presented in **Table 4** and **Figure 4**. The results of docking with the active compounds were compared to the results obtained with the known inhibitors of the targeted proteins (PMSF, TyrphostinAG1478, Auranofin, Neolignan).

Table 4. Binding energies (kcal/mol) for the molecular docking simulation of the active compounds with the schistosomes drug targets proteins.

Compounds	SmCER2a	SER	SmTGR	SmPNP
L^3	−6.1	−6.1	−8.0	−8.5
HL^2	−7.3	−7.3	−8.5	−9.5
2	−8.3	−7.9	−7.9	−10.1
Inhibitors	−4.1 PMSF (Phenylmethylsulfonyl Fluoride)	−6.7 (TyrphostinAG1478)	−7.2 (Auranofin)	−8.7 (Neolignan)

The results in **Table 4** suggest that all the active compounds have good binding affinities with the active site of the target proteins, highlighted by their low binding energies ranging from −6.1 kcal/mol to −10.1 kcal/mol. Moreover, compound 2 emerged as the best compound with strong binding affinities with very low binding energies (−8.3 (SmCE2a), −7.9 (SER), −7.9 (SmTGR), −10.1 (SmPNP) kcal/mol) across targets as compared to the two ligands. Also, SmPNP shows strong interactions with all three compounds −8.5 kcal/mol (L^3), −9.5 kcal/mol (HL^2), −10.1 kcal/mol (2). Indeed, the binding affinities of these three compounds were comparable to or stronger than that of the known inhibitors of the four targets: −4.1, −6.7, −7.2, −8.7 kcal/mol for SmCE2a-PMSF, SER-TyrphostinAG1478, SmTGR-Auranofin and SmPNP-Neolignan respectively.

The contact residues with compounds and known inhibitors in the active site of the proteins are presented in supplementary **Table S3**. The two ligands formed interactions with SmTGR through several contact residues, including CYS 154 and CYS 159, which are important amino acid residues in the active site of SmTGR responsible for the enzyme activity [82]. Furthermore, compounds L^3, HL^2 and 2 formed 3, 5 and 1 hydrogen bonds respectively with THR 158 TYR 138 ALA 256 (L^3), CYS 159 THR 442 LEU 441 ASP 443 THR 442 (HL^2) and VAL 469 (2). The greater the number of hydrogen bonds, the higher the binding efficiency and inhibition [83]. It has been demonstrated that treatment of *S. mansoni* with a TGR inhibitor resulted in 100% mortality of the parasite *in vitro*, implying that these compounds can be used against schistosomiasis [84]. The primary amino acids involved during Ligand-SmPNP interaction are CYS 33, ARG 86, HIS 88, TYR 90, ALA 118, ALA 119, PRO 200, TYR 202, GLU 203, VAL 219, MET 221, THR 244, ASN 245, PRO 257, and HIS 259. Similar interacting residues were reported [85]. 4, 4 and 2 hydrogen bond interactions with the amino acids residues MET 221, ALA 118, VAL 262, SER 35 (L^3), VAL 262, SER 35, LEU 263, HIS 259 (HL^2) and MET 221, HIS 259 (2) were formed in the active site while they have been reported to be part of important amino residues in the active site of SmPNP responsible for the enzyme activity [86]. Therefore, due to all these facts, all the active compounds may be good inhibitors of SmPNP, leading to a stop or a decrease in purine base synthesis necessary for nucleic acid synthesis and consequently the parasite death [85].

SmCE2a is another important target, an enzyme responsible for degrading skin host tissue during cercariae penetration to facilitate invasion [87]. All the compounds docked to this enzyme had lower binding energies −6.3 kcal/mol, −7.7 kcal/mol, −8.3 kcal/mol than its known inhibitor PMSF, highlighting their strong binding affinities to SmCE2a better than PMSF, which was reported to inhibit cercarial elastase *in vitro* [88]. The binding modes and interactions of ligands-SmCE2a show that the active compounds interact with the enzyme through important bond formation, including 3 hydrogen bonds with HIS 67, TYR 104, SER 217 for L^3-SmCE2a, 5 with HIS 67, TYR 107, ASP 125 for HL^2-SmCE2a and 1 with SER 217 for 2-SmCE2a, thereby contributing to the docked complexes stability

and reinforcing the binding affinity.

Schistosoma epidermal growth factor receptor SER are receptor tyrosine kinases (RTK) that represent key molecules for the development and reproductive activity processes in schistosome worms, and targeting RTK, including SER, can affect the survival of *S. mansoni* [89]. From the docking results of this enzyme, the low binding energies as compared to the known inhibitor Tyrphostin AG1478 suggest that the active compounds bind strongly to SER, added to the hydrogen bonds they formed with GLN 147, CYS 270, GLY 280, GLY 268, ASP 90, MET 277, GLY 280, that stabilise the complexes, thus could be potential inhibitors of SER. Figure 4 illustrates the binding modes and interactions identified in Table S3.

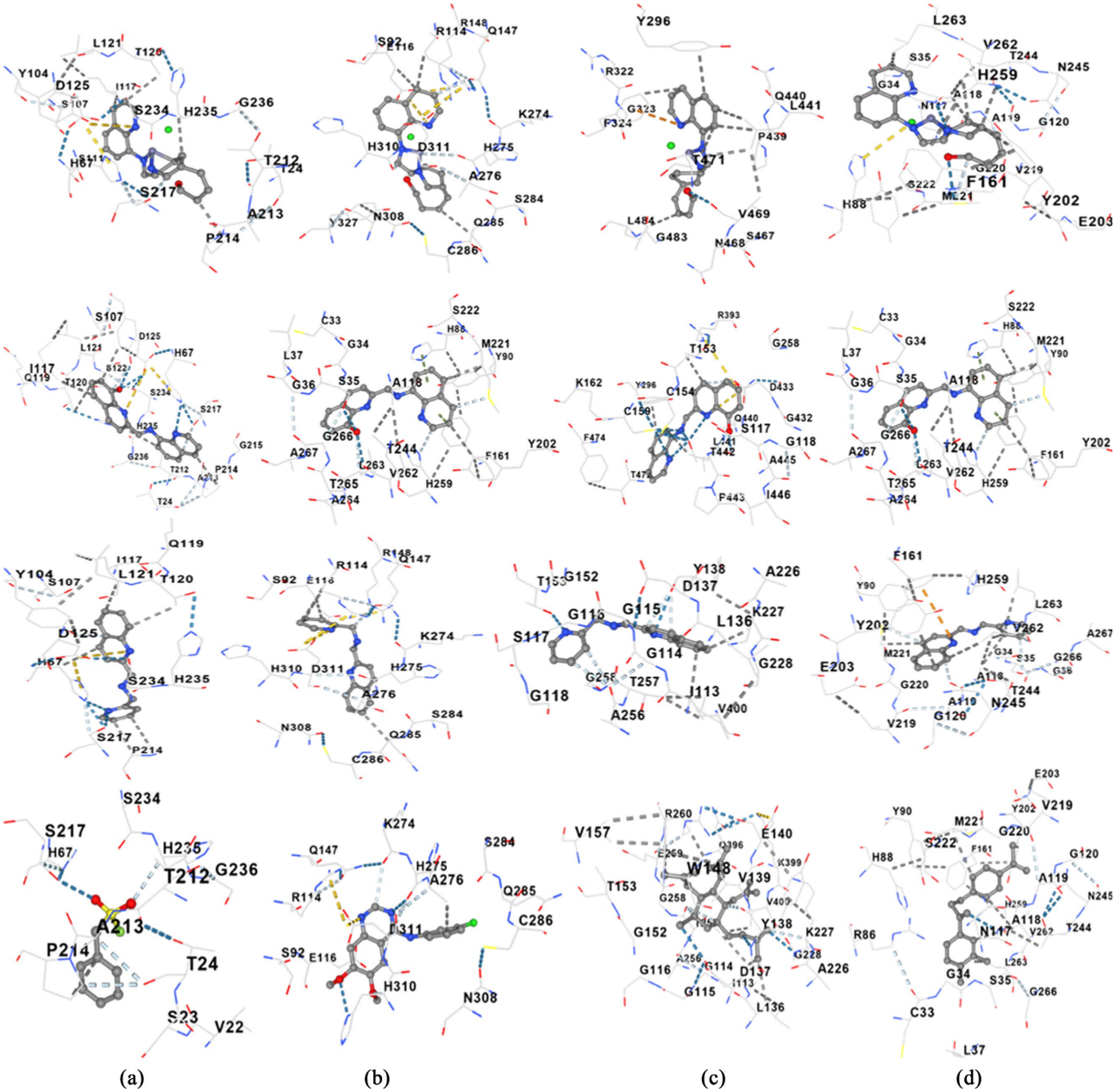

Figure 4. Docked compounds **HL²** and **L³**, **2** and **inhibitors** in the active sites of (a) SmCE2a, (b)SER, (c) SmTGR, and (d) SmPNP.

3.6. *In Silico* Physicochemical and Pharmacokinetics Predictions

After evaluating the binding affinities of the compounds with the schistosome targets, the three active compounds and Praziquantel (the drug used against schistosomiasis) were subjected to pharmacokinetic property prediction. This involved an examination of their physicochemical properties and drug-likeness characteristics. The predicted properties of active compounds and Praziquantel calculated using the SwissADME web server (http://www.swissadme.ch) and presented in Table 5 provide insights into their potential physicochemical properties, lipophilicity, water solubility, pharmacokinetics, drug likeness and medicinal chemistry profiles [90].

Table 5. Pharmacokinetic properties predictions of the active compounds.

Properties	L^3	HL^2	2	Praziquantel
Physicochemical				
Formula	$C_{16}H_{13}N_3$	$C_{19}H_{13}N_3O$	$C_{19}H_{13}ClN_3OZn$	$C_{19}H_{24}N_2O_2$
Molecular weight (g/mol)	247.29	299.33	399.15	312.41
Rotatable bonds	3	2	0	2
H-bond acceptors	3	4	1	2
H-bond donor	0	1	0	0
Molar refractivity topological polar surface area (TPSA) ($Å^2$)	77.48	92.76	100.55	96.93
Lipophilicity				
LogP *o*/*w* (ilogp)	2.19	2.90	0.00	3
LogP *o*/*w* (Xlopp3)	2.73	3.74	5.08	2.7
LogP *o*/*w* (Wlogp)	3.10	4.24	4.68	1.45
LogP *o*/*w* (Mlogp)	1.64	2.13	2.36	2.40
LogP *o*/*w* (Silicos-IT LogP)	4.17	4.32	−1.86	2.47
Concensus LogP	2.77	3.47	2.05	2.40
Water solubility				
Log S (ESOL)	Soluble	Moderately soluble	Poorly Soluble	Soluble
Log S (Ali)	Soluble	Moderately soluble	Moderately soluble	Soluble
Log S (Silicos-IT)	Poorly Soluble	Poorly Soluble	Poorly soluble	Soluble
Concensus Log S	Soluble	Moderately soluble	Poorly soluble	Soluble
Pharmacokinetics				

Continued

GI absorption	High	High	High	High
BBB permeant	Yes	Yes	Yes	Yes
P-gp substrate	No	No	Yes	Yes
CYP1A2 inhibitor	Yes	Yes	Yes	No
CYP2C19 inhibitor	Yes	Yes	No	Yes
CYP2C9 inhibitor	No	Yes	No	No
CPY2D6 inhibitor	Yes	Yes	No	Yes
CPY3A4 inhibitor	Yes	Yes	Yes	Yes
LogKp (cm/s)	−5.87	−5.47	−5.13	−6.31
Druglikeness				
Lipinski violations	0	0	0	0
Ghose violations	0	0	0	0
Veber violations	0	0	0	0
Egan violations	0	0	0	0
Bioavailability score	0.55	0.55	0.55	0.55
Medicinal chemistry				
Synthetic accessibility	2.76	2.73	3.99	2.90

The selection of new drugs and formulations is based on the physicochemical properties, which include the molecular weight, solubility, molar refractivity, topological polar surface area and hydrogen bonding capacity. These properties are essential factors for finding new drug candidates and should agree with different rule-based filters such as drug-likeness rules [90]. There are some drug-likeness rules [91] which can be described as Lipinski's rule (MW ≤ 500, Mlog P ≤ 5, H-acc ≤ 10, H-don ≤ 5); Ghose's filter (160 ≤ MW ≤ 480, −0.4 ≤ Wlog P ≤ 5.6, 40 ≤ MR ≤ 130, and 20 ≤ atoms ≤ 70); Veber's filter (R-bonds ≤ 10, and TPSA ≤ 140), and Egan's filter (Wlog P ≤ 5.88, and TPSA ≤ 131.6). Based on these rules, we found that the three active compounds agree with the four drug-likeness rules (Lipinski, Ghose, Veber, and Egan rules) and these derivatives can be accepted as lead compounds for the development of a new drug candidate [92]. A compound is like a drug if the drug-likeness score is valued positively, or the compound is non-drug if the drug-likeness score is valued negatively [93].

The drug-likeness score analysis is based on the positive and negative values of the target compounds, where the Oral drugs have fewer H-bond acceptors, donors, and rotatable bonds [94] and in the same way, compounds with a TPSA of >140 $Å^2$ would be poorly absorbed with less than 10% fractional absorption. Thus, compounds L^3, HL^2, 2 with rotatable bonds 3, 2, 0 respectively and hydrogen bond donors and acceptors < 4 fulfil all the required criteria to be well absorbed. The consensus log P o/w of the three predicted compounds of 2.77, 3.47, and 2.41 for

L^3, HL^2, and 2 respectively, indicated that the compounds are lipophilic, with HL^2 being the most lipophilic, given that a higher log Po/w value indicates higher lipophilicity and can be easily absorbed through barriers because of the lipid nature of targets [95]. Furthermore, aqueous solubility is an important parameter influencing absorption and facilitating the ease of drug handling and formulation [96]. Compound L^3 was classified as soluble, while HL^2 and 2 exhibited moderate solubility from their consensus Log S values. Interestingly, the three investigated compounds had high gastrointestinal absorptions and were blood-brain barrier permeant, meaning that they have a good absorption.

CYP enzymes and Permeability glycoprotein (P-gp) can process small molecules synergistically to improve the protection of tissues and organisms [97]. P-gp expressed in the intestinal epithelium pumps xenobiotics such as drugs back into the intestinal lumen and in the capillary endothelial cells composing the blood-brain barrier, where it pumps them back into the capillaries. While CYP P450 enzymes are responsible for drug metabolism, which can lead to drug toxicities and reduced pharmacological effect [98]. From the results, the three compounds were P-gp substrates, meaning that these compounds interact with P-gp, limiting intracellular drug accumulation in the organism. On the other hand, the compounds were either inhibitors or noninhibitors of the different isoforms of CYP P450, though it was reported that only CYP2D6 and CYP3A4 are responsible for drug metabolism [96]. Only 2 is not an inhibitor of CYP2D6, while the rest, including the reference Praziquantel, inhibited it and all the three compounds, including Praziquantel, were inhibitors of CYP3A4. Overall, SwissADME has computational filters that include Lipinski, Ghose, Egan, Veber, and were developed by leading pharmaceutical companies and computational chemist to evaluate the drug-likeness of small molecules.

Generally, drug-likeness is predicted using Lipinski (rule of five) and Veber's rules, consequently, a compound that can be used as orally active drug should not present more than one violation [99]. Lipinski's Rule of five is the pioneer filter that is associated with 90% of the oral drugs that have reached phase II clinical trials [93]. This Rule of 5 predicts that poor absorption or permeation is more likely when there are more than 5 H-bond donors, 10 H-bond acceptors, molecular weight greater than 500, and the calculated Log P (CLog P) greater than 5 [100]. From the prediction, all the compounds complied with the four rules-based filters, and no one violated any of the rules, implying these compounds could be promising lead compounds for the development of good oral drugs. Moreover, a bioavailability score of 0.55 predicts the probability of these compounds to have at least 10% oral bioavailability in rat [101]. Additionally, the medicinal chemistry shows that these compounds can be easily synthesized step by step in the laboratory, highlighted by their low synthetic accessibility scores of 2.76 (L3), 2.73 (HL^2), and 3.99 (2).

4. Conclusion

Three quinolinyl Schiff base ligands, $\mathbf{L^1}$, $\mathbf{HL^2}$ and $\mathbf{L^3}$, were synthesized, and they

acted as tridentate *NNN*- or tetradentate *NNNO*-donors. Their Zn(II) metal complexes (**1**, **2** and **3**) showed trigonal bipyramidal and square pyramidal proposed geometry based on the spectroscopic analyses. Density Functional Theory used to optimise the structure of ligands and their metal complexes was discussed. **L^3**, **HL^2** and **2** displaced very good antischistosomal activity, with compound **2** being the most active. In general, Zn(II) complex **2** shows slightly higher activity (1.14 μg/mL) than its ligand **HL^2** (1.23 μg/mL), therefore they show more promising results as lead compounds against *S. mansoni* parasite. All the active compounds were also non-cytotoxic to the Vero cell line and both HL^2 and its Zn(II) complex 2 are in similar range with good selectivity index. Furthermore, molecular docking studies clearly indicated that the active compounds exhibited good docking scores against *S. mansoni* main target enzymes, with values comparable or better than their known inhibitors. Finally, the drug-likeness prediction showed that two active Schiff bases (**L^3**, **HL^2**) and the Zn(II) complex (**2**) agree with the four drug-likeness rules (Lipinski, Ghose, Veber, and Egan rules) and these derivatives can be considered as potential lead compounds for therapeutic development against *S. mansoni* parasite.

Acknowledgements

FMM is grateful to the FAIRE programme provided by the Cambridge Crystallographic Data Centre (CCDC) for the opportunity to use the Cambridge Structural Database (CSD) and associated software.

Conflicts of Interest

The authors declare no conflicts of interest regarding the publication of this paper.

References

[1] Afrin, A. and Chinna Ayya Swamy, P. (2023) Novel Schiff Base Derivatives for the Detection of One-to-Multi Metal Ions and Tracking the Live Cell Imaging. *Coordination Chemistry Reviews*, **494**, Article ID: 215327. https://doi.org/10.1016/j.ccr.2023.215327

[2] Manna, A.K., Rout, K., Chowdhury, S. and Patra, G.K. (2019) A Dual-Mode Highly Selective and Sensitive Schiff Base Chemosensor for Fluorescent Colorimetric Detection of Ni^{2+} and Colorimetric Detection of Cu^{2+}. *Photochemical & Photobiological Sciences*, **18**, 1512-1525. https://doi.org/10.1039/c9pp00114j

[3] Khandar, A.A., Afkhami, F.A., Hosseini-Yazdi, S.A., White, J.M., Kassel, S., Dougherty, W.G., *et al.* (2015) Anion Influence in the Structural Diversity of Cadmium Coordination Polymers Constructed from a Pyridine Based Schiff Base Ligand. *Inorganica Chimica Acta*, **427**, 87-96. https://doi.org/10.1016/j.ica.2014.11.028

[4] Kajal, A., Bala, S., Kamboj, S., Sharma, N. and Saini, V. (2013) Schiff Bases: A Versatile Pharmacophore. *Journal of Catalysts*, **2013**, Article ID: 893512. https://doi.org/10.1155/2013/893512

[5] Garrido Montalban, A. (2011) Quinolines and Isoquinolines. In: Majumdar, K.C. and Chattopadhyay, S.K., Eds., *Heterocycles in Natural Products Synthesis*, Wiley-VCH, 299-339.

[6] Kouznetsov, V.V., Meléndez Gómez, C.M., Peña, J.L.V. and Vargas-Méndez, L.Y. (2019) Natural and Synthetic Quinoline Molecules against Tropical Parasitic Pathologies: An Analysis of Activity and Structural Evolution for Developing New Quinoline-Based Antiprotozoal Agents. In: Brahmachari, G., Ed., *Discovery and Development of Therapeutics from Natural Products Against Neglected Tropical Diseases*, Elsevier, 87-164. https://doi.org/10.1016/b978-0-12-815723-7.00004-3

[7] Rajesh, Y.B.R.D. (2020) Quinoline Heterocycles: Synthesis and Bioactivity. In: Nandeshwarappa, B.P. and Sadashiv, S.O., Eds., *Heterocycles-Synthesis and Biological Activities*, Intech Open, 202 p.

[8] Kumar, S., Bawa, S. and Gupta, H. (2009) Biological Activities of Quinoline Derivatives. *Mini Review of Medicinal Chemistry*, **9**, 1648-1654.

[9] Adsule, S., Barve, V., Chen, D., Ahmed, F., Dou, Q.P., Padhye, S., *et al.* (2006) Novel Schiff Base Copper Complexes of Quinoline-2 Carboxaldehyde as Proteasome Inhibitors in Human Prostate Cancer Cells. *Journal of Medicinal Chemistry*, **49**, 7242-7246. https://doi.org/10.1021/jm060712l

[10] Beyzaei, H., Hosseini Moghadam, H., Bagherzade, G., Aryan, R. and Moghaddam-Manesh, M. (2019) Synthesis and *in Vitro* Antibacterial Evaluation of Schiff Bases Derived from 2-Chloro-3-Quinolinecarboxaldehyde. *Avicenna Journal of Medical Biochemistry*, **7**, 9-15. https://doi.org/10.34172/ajmb.2019.03

[11] Sakthi, M. and Ramu, A. (2017) Synthesis, Structure, DNA/BSA Binding and Antibacterial Studies of NNO Tridentate Schiff Base Metal Complexes. *Journal of Molecular Structure*, **1149**, 727-735. https://doi.org/10.1016/j.molstruc.2017.08.040

[12] Shivakumar, L., Shivaprasad, K. and Revanasiddappa, H.D. (2013) Sods, DNA Binding and Cleavage Studies of New Mn(III) Complexes with 2-((3-(Benzyloxy)pyridin-2-Ylimino)methyl)phenol. *Spectrochimica Acta Part A*: *Molecular and Biomolecular Spectroscopy*, **107**, 203-212. https://doi.org/10.1016/j.saa.2013.01.025

[13] Boussadia, A., Beghidja, A., Gali, L., Beghidja, C., Elhabiri, M., Rabu, P., *et al.* (2020) Coordination Properties of Two New Schiff-Base Phenoxy-Carboxylates and Comparative Study of Their Antioxidant Activities. *Inorganica Chimica Acta*, **508**, Article ID: 119656. https://doi.org/10.1016/j.ica.2020.119656

[14] Wang, F., Tang, X., Wang, X., Huang, K., Feng, H., Chen, Z., *et al.* (2018) Mitochondria-Targeted Platinum(II) Complexes Induce Apoptosis-Dependent Autophagic Cell Death Mediated by ER-Stress in A549 Cancer Cells. *European Journal of Medicinal Chemistry*, **155**, 639-650. https://doi.org/10.1016/j.ejmech.2018.06.018

[15] Ribeiro, N., Farinha, P.F., Pinho, J.O., Luiz, H., Mészáros, J.P., Galvão, A.M., *et al.* (2022) Metal Coordination and Biological Screening of a Schiff Base Derived from 8-Hydroxyquinoline and Benzothiazole. *Pharmaceutics*, **14**, Article 2583. https://doi.org/10.3390/pharmaceutics14122583

[16] Sun, W., Wang, K., Wedeking, K., Zhang, D., Zhang, S., Cai, J., *et al.* (2007) Synthesis, Characterization, and Ethylene Oligomerization of Nickel Complexes Bearing *N*-((Pyridin-2-yl)methylene)quinolin-8-amine Derivatives. *Organometallics*, **26**, 4781-4790. https://doi.org/10.1021/om700440v

[17] Ghorai, P., Brandão, P., Benmansour, S., García, C.J.G. and Saha, A. (2020) Azido and Thiocyanato Bridged Dinuclear Ni(II) Complexes Involving 8-Aminoquinoline Based Schiff Base as Blocking Ligands: Crystal Structures, Ferromagnetic Properties and Magneto-Structural Correlations. *Polyhedron*, **188**, Article ID: 114708. https://doi.org/10.1016/j.poly.2020.114708

[18] Kurdekar, G.S., Mudigoudar Puttanagouda, S., Kulkarni, N.V., Budagumpi, S. and

Revankar, V.K. (2010) Synthesis, Characterization, Antibiogram and DNA Binding Studies of Novel Co(II), Ni(II), Cu(II), and Zn(II) Complexes of Schiff Base Ligands with Quinoline Core. *Medicinal Chemistry Research*, **20**, 421-429. https://doi.org/10.1007/s00044-010-9330-5

[19] Turan, N., Buldurun, K., Alan, Y., Savci, A., Çolak, N. and Mantarcı, A. (2019) Synthesis, Characterization, Antioxidant, Antimicrobial and DNA Binding Properties of Ruthenium(II), Cobalt(II) and Nickel(II) Complexes of Schiff Base Containing O-Vanillin. *Research on Chemical Intermediates*, **45**, 3525-3540. https://doi.org/10.1007/s11164-019-03806-3

[20] Yang, Q., Cao, Q., Qin, Q., Deng, C., Liang, H. and Chen, Z. (2018) Syntheses, Crystal Structures, and Antitumor Activities of Copper(II) and Nickel(II) Complexes with 2-((2-(Pyridin-2-yl)hydrazono)methyl)quinolin-8-ol. *International Journal of Molecular Sciences*, **19**, Article 1874. https://doi.org/10.3390/ijms19071874

[21] Adeleke, A.A., Zamisa, S.J., Islam, M.S., Olofinsan, K., Salau, V.F., Mocktar, C., *et al.* (2021) Quinoline Functionalized Schiff Base Silver (I) Complexes: Interactions with Biomolecules and *in Vitro* Cytotoxicity, Antioxidant and Antimicrobial Activities. *Molecules*, **26**, Article 1205. https://doi.org/10.3390/molecules26051205

[22] Lu, W., Chen, J., Shi, J., Xu, L., Yang, S. and Gao, B. (2021) A Novel Quinoline-Based Turn-On Fluorescent Probe for the Highly Selective Detection of Al (III) and Its Bioimaging in Living Cells, Plants Tissues and Zebrafish. *JBIC Journal of Biological Inorganic Chemistry*, **26**, 57-66. https://doi.org/10.1007/s00775-020-01836-6

[23] Kumar Raju, S., Settu, A., Thiyagarajan, A., Rama, D., Sekar, P. and Kumar, S. (2022) Biological Applications of Schiff Bases: An Overview. *GSC Biological and Pharmaceutical Sciences*, **21**, 203-215. https://doi.org/10.30574/gscbps.2022.21.3.0484

[24] WHO (2021) Schistosomiasis and Soil Transmitted Helminthiases: Progress Report. *Weekly Epidemiological Record*, **97**, 621-632. http://www.who.int/wer

[25] Asante-Kwatia, E., Gyimah, L., Forkuo, A.D., Anyan, W.K., Gbemu, M.A., Armah, F.A., *et al.* (2023) Ethnobotanical Survey and Cercaricidal Activity Screening of Medicinal Plants Used for Schistosomiasis Treatment in Atwima-Nwabiagya District, Ashanti Region, Ghana. *Journal of Parasitology Research*, **2023**, Article ID: 6707157. https://doi.org/10.1155/2023/6707157

[26] Azevedo, C.M., Meira, C.S., da Silva, J.W., Moura, D.M.N., de Oliveira, S.A., da Costa, C.J., *et al.* (2023) Therapeutic Potential of Natural Products in the Treatment of Schistosomiasis. *Molecules*, **28**, Article 6807. https://doi.org/10.3390/molecules28196807

[27] Fenwick, A. and Jourdan, P. (2016) Schistosomiasis Elimination by 2020 or 2030? *International Journal for Parasitology*, **46**, 385-388. https://doi.org/10.1016/j.ijpara.2016.01.004

[28] French, M.D., Evans, D., Fleming, F.M., Secor, W.E., Biritwum, N., Brooker, S.J., *et al.* (2018) Schistosomiasis in Africa: Improving Strategies for Long-Term and Sustainable Morbidity Control. *PLOS Neglected Tropical Diseases*, **12**, e0006484. https://doi.org/10.1371/journal.pntd.0006484

[29] Olorunlana, A. (2022) Dancing in a Cycle: Global Health Agenda and *Schistosomiasis* Control in Africa. In: Morales-Montor, J., Del Río-Araiza, V.H. and Hernandéz-Bello, R., Eds., *Parasitic Helminths and Zoonoses—From Basic to Applied Research*, IntechOpen, 400 p. https://doi.org/10.5772/intechopen.103164

[30] Ross, A.G.P., Olveda, R.M. and Li, Y. (2015) An Audacious Goal: The Elimination of Schistosomiasis in Our Lifetime through Mass Drug Administration. *The Lancet*, **385**, 2220-2221. https://doi.org/10.1016/s0140-6736(14)61417-3

[31] Olveda, D.U., McManus, D.P. and Ross, A.G.P. (2016) Mass Drug Administration and the Global Control of Schistosomiasis: Successes, Limitations and Clinical Outcomes. *Current Opinion in Infectious Diseases*, **29**, 595-608. https://doi.org/10.1097/qco.0000000000000312

[32] Doenhoff, M.J., Kusel, J.R., Coles, G.C. and Cioli, D. (2002) Resistance of *Schistosoma mansoni* to Praziquantel: Is There a Problem? *Transactions of the Royal Society of Tropical Medicine and Hygiene*, **96**, 465-469. https://doi.org/10.1016/s0035-9203(02)90405-0

[33] Danso-Appiah, A. and De Vlas, S.J. (2002) Interpreting Low Praziquantel Cure Rates of *Schistosoma mansoni* Infections in Senegal. *Trends in Parasitology*, **18**, 125-129. https://doi.org/10.1016/s1471-4922(01)02209-7

[34] Ismail, M., Botros, S., Metwally, A., William, S., Farghally, A., Tao, L.F., *et al.* (1999) Resistance to Praziquantel: Direct Evidence from *Schistosoma mansoni* Isolated from Egyptian Villagers. *The American Journal of Tropical Medicine and Hygiene*, **60**, 932-935. https://doi.org/10.4269/ajtmh.1999.60.932

[35] WHO (2020) Ending the Neglect to Attain the Sustainable Development Goals: A Road Map for Neglected Tropical Diseases 2021-2030. World Health Organization, 41. https://www.who.int/publications/i/item/9789240010352

[36] Bergquist, R., Utzinger, J. and Keiser, J. (2017) Controlling Schistosomiasis with Praziquantel: How Much Longer without a Viable Alternative? *Infectious Diseases of Poverty*, **6**, Article No. 74. https://doi.org/10.1186/s40249-017-0286-2

[37] Qokoyi, N.K., Masamba, P. and Kappo, A.P. (2021) Proteins as Targets in Anti-Schistosomal Drug Discovery and Vaccine Development. *Vaccines*, **9**, Article 762. https://doi.org/10.3390/vaccines9070762

[38] Oliveira, T.A.S., Zago, M.H.M., Maciel, L.G., Robles, Y.R., Magalhães, L.G. and Crotti, A.E.M. (2026) Antischistosomal Activity of 1,4-Dihydropyridines. *Drugs and Drug Candidates*, **5**, Article 8. https://doi.org/10.3390/ddc5010008

[39] Paixão, V.V.M., Santos, Y.J.A., Fernandes, A.O., Conceição, E.S., Rodrigues, R.P., Chagas-Paula, D.A., *et al.* (2025) Novel Antischistosomal Drug Targets: Identification of Alkaloid Inhibitors of Smtgr via Integrated *in Silico* Methods. *Pathogens*, **14**, Article 591. https://doi.org/10.3390/pathogens14060591

[40] Gambino, D. (2024) Organometallics in Medicinal Chemistry: Antiparasitic Agents. *Journal of the Brazilian Chemical Society*, **35**, e-20240104. https://doi.org/10.21577/0103-5053.20240104

[41] Vitali, V., Zineddu, S. and Messori, L. (2025) Metal Compounds as Antimicrobial Agents: 'Smart' Approaches for Discovering New Effective Treatments. *RSC Advances*, **15**, 748-753. https://doi.org/10.1039/d4ra07449a

[42] de Moraes, J., Dario, B.S., Couto, R.A.A., Pinto, P.L.S. and da Costa Ferreira, A.M. (2015) Antischistosomal Activity of Oxindolimine-Metal Complexes. *Antimicrobial Agents and Chemotherapy*, **59**, 6648-6652. https://doi.org/10.1128/aac.01371-15

[43] Portes, M.C., Ribeiro, G.A., Sabino, G.L., De Couto, R.A.A., Vieira, L.Q., Alves, M.J.M., *et al.* (2023) Antiparasitic Activity of Oxindolimine-Metal Complexes against Chagas Disease. *Inorganics*, **11**, Article 420. https://doi.org/10.3390/inorganics11110420

[44] Moreira, G., Lima, C., Andrade, D., Rego, N., Passos, I., de Moraes, J., Lima, F. and Rocha, J. (2020) Study of Metal Complexes of Ruthenium against Schistosomosis: A Scientific and Technological Prospection. *Journal of Global Innovation*, **2**, 1-11.

[45] Majoumo-Mbe, F., Nono, J.H., Sangbong, N.A. and Efeti, I.I. (2024) Synthesis, Spectroscopic Characterization, DFT Analysis and Molecular Docking of Mn(II), Co(II)

and Ni(II) Complexes of Hydrazone Derived from 5-Chloroisatin and 2,4-Dinitrophenylhydrazine. *Journal of Organometallic Chemistry*, **1013**, Article ID: 123184. https://doi.org/10.1016/j.jorganchem.2024.123184

[46] Majoumo-Mbe, F., Sangbong, N.A., Tadjong Tcho, A., Namba-Nzanguim, C.T., Simoben, C.V., Eni, D.B., *et al.* (2024) 5-Chloro-3-(2-(2,4-Dinitrophenyl) Hydrazono)indolin-2-One: Synthesis, Characterization, Biochemical and Computational Screening against SARS-CoV-2. *Chemical Papers*, **78**, 3431-3441. https://doi.org/10.1007/s11696-023-03274-5

[47] Effeti, I.I., Majoumo-Mbe, F., Louis, H., Nfor, E.N., Akongwi, M., Unimuke, T.O., *et al.* (2023) Modeling of Photofunctional Transition Metals (Mn, Re, Ir) Complexes Towards the Effective Detection of Uric Acid (UA) as Biomarker for Kidney Dysfunction. *Journal of Photochemistry and Photobiology A*: *Chemistry*, **444**, Article ID: 114942. https://doi.org/10.1016/j.jphotochem.2023.114942

[48] Majoumo-Mbe, F., Ngwang Nfor, E., Kenfack Tsobnang, P., Nguepmeni Eloundou, V.B., Ngwain Yong, J. and Iris Efeti, I. (2019) Synthesis, Molecular and Crystal Structure of 1-(1,2-Dihydrophthalazin-1-ylidene)-2-[1-(thiophen-2-yl)ethylidene]hydrazine. *Acta Crystallographica Section e Crystallographic Communications*, **75**, 251-254. https://doi.org/10.1107/s2056989019000732

[49] Yong, J.N., Majoumo-Mbe, F., Samje, M. and Nfor, E.N. (2016) Synthesis, Molecular Structure and Anti-Onchocercal Studies of 1-(Phthalazin-1(2H)-one)[(Pyridin-2-yl)ethylidene]hydrazone. *International Journal of Organic Chemistry*, **6**, 77-84. https://doi.org/10.4236/ijoc.2016.61008

[50] Majoumo-Mbe, F., Nfor, E. N., Sengeh, E. B., Njong, R. N. and Offiong, O. E. (2015) Synthesis, Crystal Structure and Biological Activity of 1-(Phthalazin-1(2H)-one)[(Pyridin-2-yl)ethylidene]hydrazone and Its Cobalt (III) Complex. *Communications in Inorganic Synthesis*, **3**, 40-46.

[51] Nfor, E.N., Husian, A., Majoumo-Mbe, F., Njah, I.N., Offiong, O.E. and Bourne, S.A. (2013) Synthesis, Crystal Structure and Antifungal Activity of a Ni(II) Complex of a New Hydrazone Derived from Antihypertensive Drug Hydralazine Hydrochloride. *Polyhedron*, **63**, 207-213. https://doi.org/10.1016/j.poly.2013.07.028

[52] Roy, N., Pramanik, H.A.R., Paul, P.C. and Singh, T.S. (2015) A Highly Sensitive and Selective Fluorescent Chemosensor for Detection of Zn^{2+} Based on a Schiff Base. *Spectrochimica Acta Part A*: *Molecular and Biomolecular Spectroscopy*, **140**, 150-155. https://doi.org/10.1016/j.saa.2014.12.106

[53] Dongmo Nguepi, M.S., Itoe, U.S., Itoe, F.A., Woutouoba Ntieche, D., Dize, D., Kemzeu, R., *et al.* (2024) Persea Americana, Curcuma Longa and Allium Sativum Extracts Exhibit Cercaricidal, Anti-Inflammatory and Anti-Oxidant Activities. *South African Journal of Botany*, **169**, 268-275. https://doi.org/10.1016/j.sajb.2024.04.024

[54] Balbaied, T. and Moore, E. (2020) Resazurin-Based Assay for Quantifying Living Cells during Alkaline Phosphatase (ALP) Release. *Applied Sciences*, **10**, Article 3840. https://doi.org/10.3390/app10113840

[55] Bickelhaupt, F.M. and Baerends, E. J. (2000) Kohn-Sham Density Functional Theory: Predicting and Understanding Chemistry. In: Lipkowitz, K.B. and Boyd, D.B., Eds, *Reviews in Computational Chemistry*, Wiley-VCH, Inc., 1-86.

[56] Nagy, B. and Jensen, F. (2017) Basis Sets in Quantum Chemistry. *Reviews in Computational Chemistry*, **30**, 93-149.

[57] Grimme, S., Antony, J., Ehrlich, S. and Krieg, H. (2010) A Consistent and Accurateab Initioparametrization of Density Functional Dispersion Correction (DFT-D) for the 94 Elements H-Pu. *The Journal of Chemical Physics*, **132**, Article ID: 154104.

https://doi.org/10.1063/1.3382344

[58] Frisch, M.J., Trucks, G.W., Schlegel, H.B., Scuseria, G.E, Robb, M.A., Cheeseman, J.R., *et al.* (2016) Gaussian 16, Revision C.01. Gaussian Inc.

[59] Dennington, R., Keith, T.A. and Millam, J.M. (2016) GaussView. Semichem Inc.

[60] Wick, C.R. and Clark, T. (2018) On Bond-Critical Points in QTAIM and Weak Interactions. *Journal of Molecular Modeling*, **24**, Article No. 142. https://doi.org/10.1007/s00894-018-3684-x

[61] Boto, R.A., Contreras-García, J., Tierny, J. and Piquemal, J. (2015) Interpretation of the Reduced Density Gradient. *Molecular Physics*, **114**, 1406-1414. https://doi.org/10.1080/00268976.2015.1123777

[62] Gadre, S.R., Suresh, C.H. and Mohan, N. (2021) Electrostatic Potential Topology for Probing Molecular Structure, Bonding and Reactivity. *Molecules*, **26**, Article 3289. https://doi.org/10.3390/molecules26113289

[63] Masnabadi, N., Thalji, M.R., Alhasan, H.S., Mahmoodi, Z., Soldatov, A.V. and Ali, G.A.M. (2022) Structural, Electronic, Reactivity, and Conformational Features of 2,5,5-Trimethyl-1,3,2-Diheterophosphinane-2-Sulfide, and Its Derivatives: DFT, MEP, and NBO Calculations. *Molecules*, **27**, Article 4011. https://doi.org/10.3390/molecules27134011

[64] Domingo, L., Ríos-Gutiérrez, M. and Pérez, P. (2016) Applications of the Conceptual Density Functional Theory Indices to Organic Chemistry Reactivity. *Molecules*, **21**, Article 748. https://doi.org/10.3390/molecules21060748

[65] Pal, R. and Chattaraj, P.K. (2021) Chemical Reactivity from a Conceptual Density Functional Theory Perspective. *Journal of the Indian Chemical Society*, **98**, Article ID: 100008. https://doi.org/10.1016/j.jics.2021.100008

[66] Kumar, P., A, A., M, M., Dangi, V., J, J. and Arya, B. (2024) A Conceptual DFT Based Analysis of Thermodynamic and Global Reactivity Parameter Indices for Pyrogallol Based Complex with Al^{3+}, Cr^{3+} and Fe^{3+} Metal Ions. *Oriental Journal of Chemistry*, **40**, 428-436. https://doi.org/10.13005/ojc/400214

[67] Dolinsky, T.J., Czodrowski, P., Li, H., Nielsen, J.E., Jensen, J.H., Klebe, G., *et al.* (2007) PDB2PQR: Expanding and Upgrading Automated Preparation of Biomolecular Structures for Molecular Simulations. *Nucleic Acids Research*, **35**, W522-W525. https://doi.org/10.1093/nar/gkm276

[68] Gomes, L.M.F., Vieira, R.P., Jones, M.R., Wang, M.C.P., Dyrager, C., Souza-Fagundes, E.M., *et al.* (2014) 8-Hydroxyquinoline Schiff-Base Compounds as Antioxidants and Modulators of Copper-Mediated Aβ Peptide Aggregation. *Journal of Inorganic Biochemistry*, **139**, 106-116. https://doi.org/10.1016/j.jinorgbio.2014.04.011

[69] González, D., Arrué, R., Matamala-Cea, E., Arancibia, R., Hamon, P., Cador, O., *et al.* (2018) Homoleptic Co^{II}, Ni^{II}, Cu^{II}, and Zn^{II} Complexes Based on 8-Hydroxylquinoline Schiff Base Derivative: A Combined Synthetic, Spectral, Structural, and Magnetic Study. *European Journal of Inorganic Chemistry*, **43**, 4720-4730. https://doi.org/10.1002/ejic.201801160

[70] Pinchaipat, B., Chotima, R., Promkatkaew, M., Kitjaruwankul, S., Chainok, K. and Khudkham, T. (2024) Experimental and Theoretical Studies on DNA Binding and Anticancer Activity of Nickel(II) and Zinc(II) Complexes with N-(8-Quinolyl) Salicylaldimine Schiff Base Ligands. *Chemistry*, **6**, 618-639. https://doi.org/10.3390/chemistry6040037

[71] Cipurković, A., Horozić, E., Marić, S., Mekić, L. and Junuzović, H. (2021) Metal Complexes with 8-Hydroxyquinoline: Synthesis and *in Vitro* Antimicrobial Activity. *Open*

Journal of Applied Sciences, **11**, 1-10. https://doi.org/10.4236/ojapps.2021.111001

[72] Ababei, L.V., Kriza, A., Andronescu, C. and Musuc, A.M. (2011) Synthesis and Characterization of New Complexes of Some Divalent Transition Metals with 2-Acetylpyridyl-Isonicotinoylhydrazone. *Journal of Thermal Analysis and Calorimetry*, **107**, 573-584. https://doi.org/10.1007/s10973-011-1457-1

[73] Ray, A., Banerjee, S., Sen, S., Butcher, R.J., Rosair, G.M., Garland, M.T., *et al.* (2007) Two Zn(II) and One Mn(II) Complexes Using Two Different Hydrazone Ligands: Spectroscopic Studies and Structural Aspects. *Structural Chemistry*, **19**, 209-217. https://doi.org/10.1007/s11224-007-9274-7

[74] Geary, W.J. (1971) The Use of Conductivity Measurements in Organic Solvents for the Characterisation of Coordination Compounds. *Coordination Chemistry Reviews*, **7**, 81-122. https://doi.org/10.1016/s0010-8545(00)80009-0

[75] Nibret, E., Ashour, M.L., Rubanza, C.D. and Wink, M. (2010) Screening of Some Tanzanian Medicinal Plants for Their Trypanocidal and Cytotoxic Activities. *Phytotherapy Research*, **24**, 945-947. https://doi.org/10.1002/ptr.3066

[76] Khan, M.O.F., Keiser, J., Amoyaw, P.N.A., Hossain, M.F., Vargas, M., Le, J.G., *et al.* (2016) Discovery of Antischistosomal Drug Leads Based on Tetraazamacrocyclic Derivatives and Their Metal Complexes. *Antimicrobial Agents and Chemotherapy*, **60**, 5331-5336. https://doi.org/10.1128/aac.00778-16

[77] Suffness, M. and Pezzuto, J.M. (1991) Assays Related to Cancer Drug Discovery. In: Hostettmann, K., Ed., *Methods in Plant Biochemistry*: *Assays for Bioactivity*, Vol. 6, Academic Press, 71-133.

[78] Serrano-Vega, R., Pérez-Gutiérrez, S., Alarcón-Aguilar, F., Almanza-Pérez, J., Pérez-González, C. and González-Chávez, M.M. (2021) Phytochemical Composition, Anti-Inflammatory and Cytotoxic Activities of Chloroform Extract of *Senna crotalarioides* Kunth. *American Journal of Plant Sciences*, **12**, 887-900. https://doi.org/10.4236/ajps.2021.126059

[79] Johnson, E.R., Keinan, S., Mori-Sánchez, P., Contreras-García, J., Cohen, A.J. and Yang, W. (2010) Revealing Noncovalent Interactions. *Journal of the American Chemical Society*, **132**, 6498-6506. https://doi.org/10.1021/ja100936w

[80] Adejumo, T.T., Tzouras, N.V., Zorba, L.P., Radanović, D., Pevec, A., Grubišić, S., *et al.* (2020) Synthesis, Characterization, Catalytic Activity, and DFT Calculations of Zn(II) Hydrazone Complexes. *Molecules*, **25**, Article 4043. https://doi.org/10.3390/molecules25184043

[81] Politzer, P. and Murray, J.S. (2021) Molecular Electrostatic Potentials: Significance and Applications. In: Chattaraj, P.K. and Chakraborty, D., Eds, *Chemical Reactivity in Confined Systems*, John Wiley & Sons, 113-134.

[82] Angelucci, F., Miele, A.E., Boumis, G., Dimastrogiovanni, D., Brunori, M. and Bellelli, A. (2008) Glutathione Reductase and Thioredoxin Reductase at the Crossroad: The Structure of *Schistosoma mansoni* Thioredoxin Glutathione Reductase. *Proteins*: *Structure*, *Function*, *and Bioinformatics*, **72**, 936-945. https://doi.org/10.1002/prot.21986

[83] Shivanika, C., Deepak Kumar, S., Ragunathan, V., Tiwari, P., Sumitha, A. and Brindha Devi, P. (2020) Molecular Docking, Validation, Dynamics Simulations, and Pharmacokinetic Prediction of Natural Compounds against the SARS-CoV-2 Main-Protease. *Journal of Biomolecular Structure and Dynamics*, **40**, 585-611. https://doi.org/10.1080/07391102.2020.1815584

[84] Eweas, A., Allam, G., Abu-Elsaad, A., Maghrabi, I. and ALGhamdi, A. (2012) Synthesis,

Anti-Schistosomal Activity and Molecular Modeling of Two Novel 8-Hydroxyquinoline Derivatives. *Anti-Infective Agents*, **11**, 31-40. https://doi.org/10.2174/22113626130104

[85] Mtemeli, F.L., Shoko, R., Ndlovu, J. and Mugumbate, G. (2022) *In Silico* Study of *Cucurbita maxima* Compounds as Potential Therapeutics against Schistosomiasis. *Bioinformatics and Biology Insights*, **16**, 1-10.

[86] D'Muniz Pereira, H., Oliva, G. and Garratt, R.C. (2010) Purine Nucleoside Phosphorylase from *Schistosoma mansoni* in Complex with Ribose-1-Phosphate. *Journal of Synchrotron Radiation*, **18**, 62-65. https://doi.org/10.1107/s0909049510027718

[87] Ingram, J.R., Rafi, S.B., Eroy-Reveles, A.A., Ray, M., Lambeth, L., Hsieh, I., *et al.* (2012) Investigation of the Proteolytic Functions of an Expanded Cercarial Elastase Gene Family in *Schistosoma mansoni*. *PLOS Neglected Tropical Diseases*, **6**, e1589. https://doi.org/10.1371/journal.pntd.0001589

[88] Bahgat, M. and Ruppel, A. (2002) Biochemical Comparison of the Serine Protease (Elastase) Activities in Cercarial Secretions from *Trichobilharzia ocellata* and *Schistosoma mansoni*. *Parasitology Research*, **88**, 495-500. https://doi.org/10.1007/s00436-002-0597-4

[89] Morel, M., Vanderstraete, M., Hahnel, S., Grevelding, C.G. and Dissous, C. (2014) Receptor Tyrosine Kinases and Schistosome Reproduction: New Targets for Chemotherapy. *Frontiers in Genetics*, **5**, Article 238. https://doi.org/10.3389/fgene.2014.00238

[90] Naglah, A.M., Askar, A.A., Hassan, A.S., Khatab, T.K., Al-Omar, M.A. and Bhat, M.A. (2020) Biological Evaluation and Molecular Docking with *in Silico* Physicochemical, Pharmacokinetic and Toxicity Prediction of Pyrazolo[1,5-*a*]pyrimidines. *Molecules*, **25**, Article 1431. https://doi.org/10.3390/molecules25061431

[91] Al Wasidi, A.S., Hassan, A.S. and Naglah, A.M. (2020) *In Vitro* Cytotoxicity and Druglikeness of Pyrazolines and Pyridines Bearing Benzofuran Moiety. *Journal of Applied Pharmaceutical Science*, **10**, 142-148.

[92] Hassan, A.S., Morsy, N.M., Aboulthana, W.M. and Ragab, A. (2023) Exploring Novel Derivatives of Isatin-Based Schiff Bases as Multi-Target Agents: Design, Synthesis, *in Vitro* Biological Evaluation, and *in Silico* ADMET Analysis with Molecular Modeling Simulations. *RSC Advances*, **13**, 9281-9303. https://doi.org/10.1039/d3ra00297g

[93] Gad, E.M., Nafie, M.S., Eltamany, E.H., Hammad, M.S.A.G., Barakat, A. and Boraei, A.T.A. (2020) Discovery of New Apoptosis-Inducing Agents for Breast Cancer Based on Ethyl 2-Amino-4,5,6,7-Tetra Hydrobenzo[*b*]Thiophene-3-Carboxylate: Synthesis, *in Vitro*, and *in Vivo* Activity Evaluation. *Molecules*, **25**, Article 2523. https://doi.org/10.3390/molecules25112523

[94] Ahmad, I., Khan, H., Usman Amin, M., Khalid, S., Behl, T. and Ur Rahman, N. (2021) An Overview on the Anticancer Potential of Punarnavine: Prediction of Drug-Like Properties. *Oncologie*, **23**, 321-333. https://doi.org/10.32604/oncologie.2021.018296

[95] Sardar, H. (2023) Drug Like Potential of Daidzein Using SwissADME Prediction: *In Silico* Approaches. *Phytonutrients*, **2**, 2-8.

[96] Mvondo, J.G.M., Matondo, A., Mawete, D.T., Bambi, S.N., Mbala, B.M. and Lohohola, P.O. (2021) *In Silico* ADME/T Properties of Quinine Derivatives Using SwissADME and pkCSM Webservers. *International Journal of Tropical Disease & Health*, **42**, 1-12. https://doi.org/10.9734/ijtdh/2021/v42i1130492

[97] Daina, A., Michielin, O. and Zoete, V. (2017) SwissADME: A Free Web Tool to Evaluate Pharmacokinetics, Drug-Likeness and Medicinal Chemistry Friendliness of Small

Molecules. *Scientific Reports*, **7**, Article No. 42717.
https://doi.org/10.1038/srep42717

[98] Ndombera, F., Maiyoh, G. and Tuei, V. (2019) Pharmacokinetic, Physicochemical and Medicinal Properties of N-Glycoside Anti-Cancer Agent More Potent than 2-Deoxy-D-Glucose in Lung Cancer Cells. *Journal of Pharmacy and Pharmacology*, **7**, 165-176.
https://doi.org/10.17265/2328-2150/2019.04.003

[99] Kekessie, F.K., Amengor, C.D.K., Brobbey, A., Addotey, J.N., Danquah, C.A., Peprah, P., *et al.* (2021) Synthesis, Molecular Docking Studies and ADME Prediction of Some New Triazoles as Potential Antimalarial Agents. *Scientific African*, **14**, e00998.
https://doi.org/10.1016/j.sciaf.2021.e00998

[100] Benet, L.Z., Hosey, C.M., Ursu, O. and Oprea, T.I. (2016) BDDCS, the Rule of 5 and Drugability. *Advanced Drug Delivery Reviews*, **101**, 89-98.
https://doi.org/10.1016/j.addr.2016.05.007

[101] Khare, S., Chatterjee, T., Gupta, S. and Ashish, P. (2023) Bioavailability Predictions, Pharmacokinetics and Drug-Likeness of Bioactive Compounds from Andrographis Paniculata Using Swiss ADME. *MGM Journal of Medical Sciences*, **10**, 651-659.
https://doi.org/10.4103/mgmj.mgmj_245_23

Supplementary Information

(L^1)

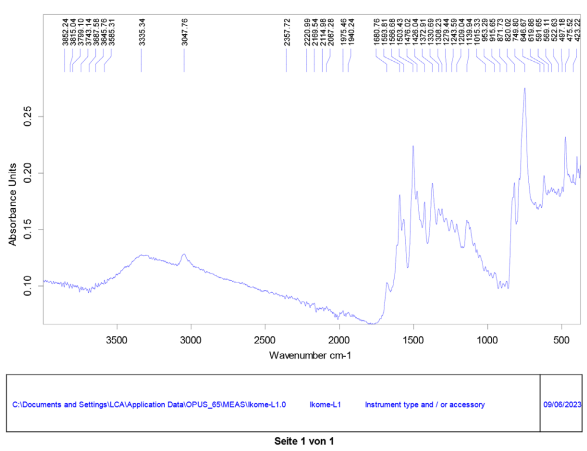

(**1**)

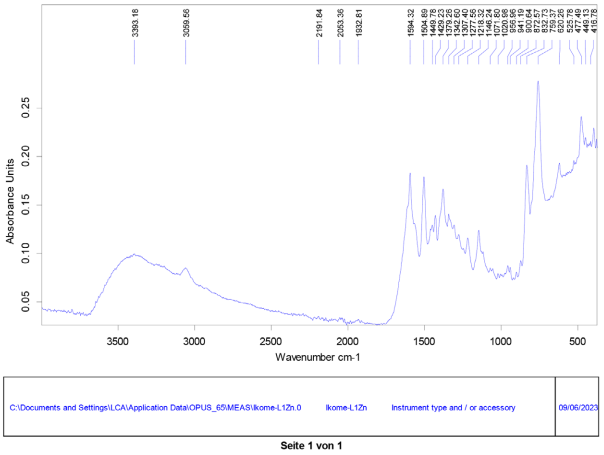

(**2**)

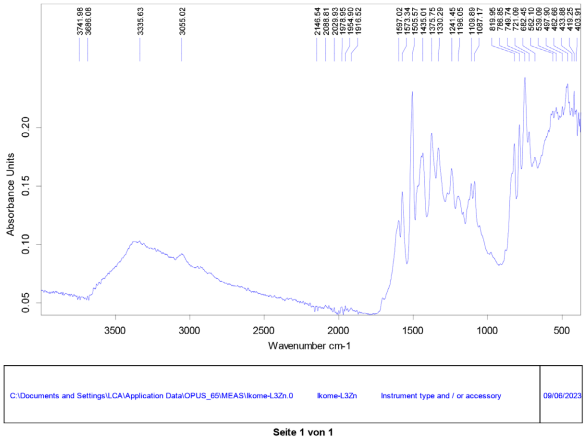

(L^3)

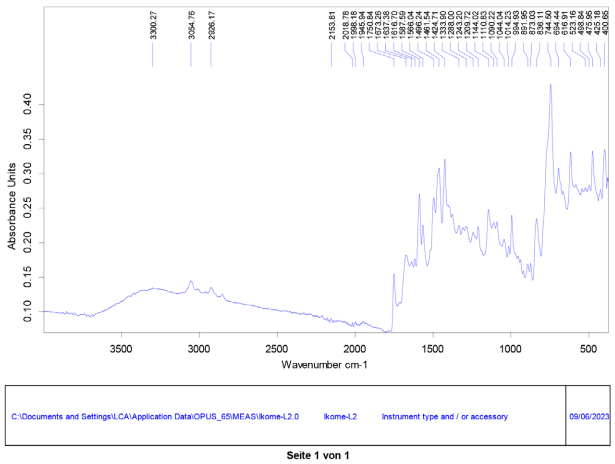

(**3**)

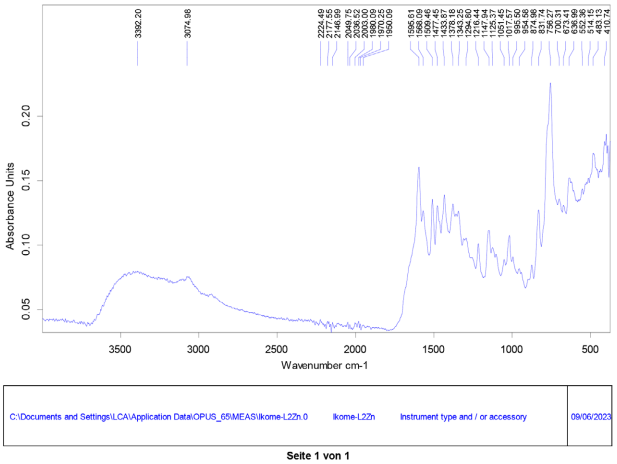

Figure S1. IR spectrum of ligands and Zn(II) complexes.

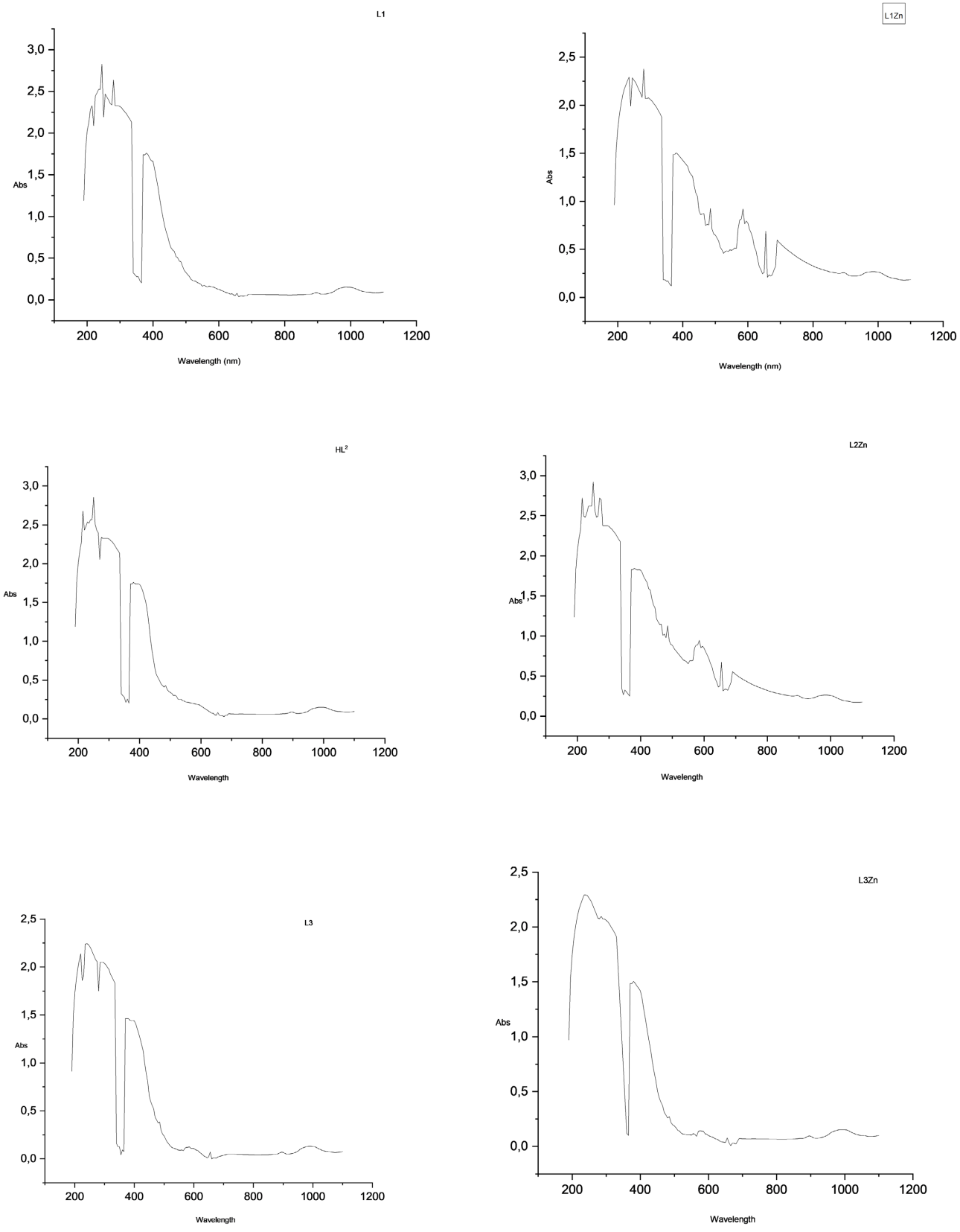

Figure S2. Electronic spectra of ligands and Zn(II) complexes.

TGA of L2Zn

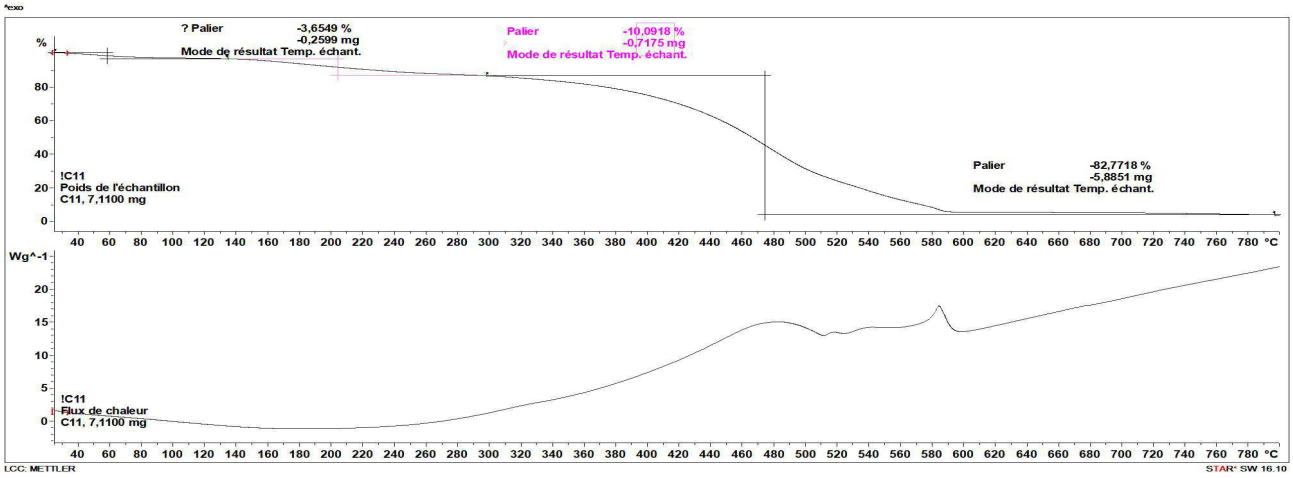

TGA of L1Zn

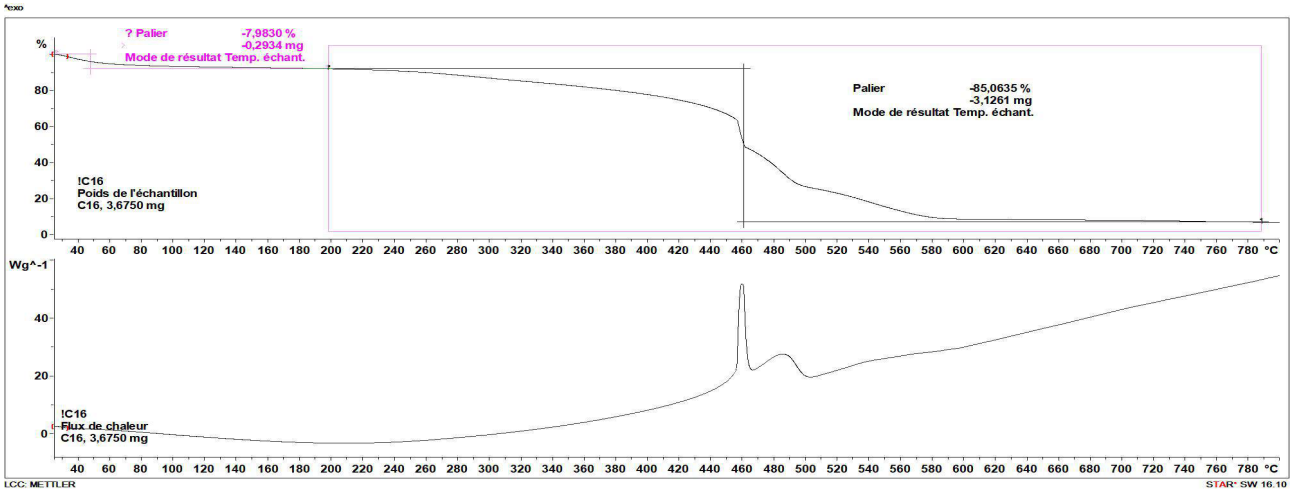

TGA of L3Zn

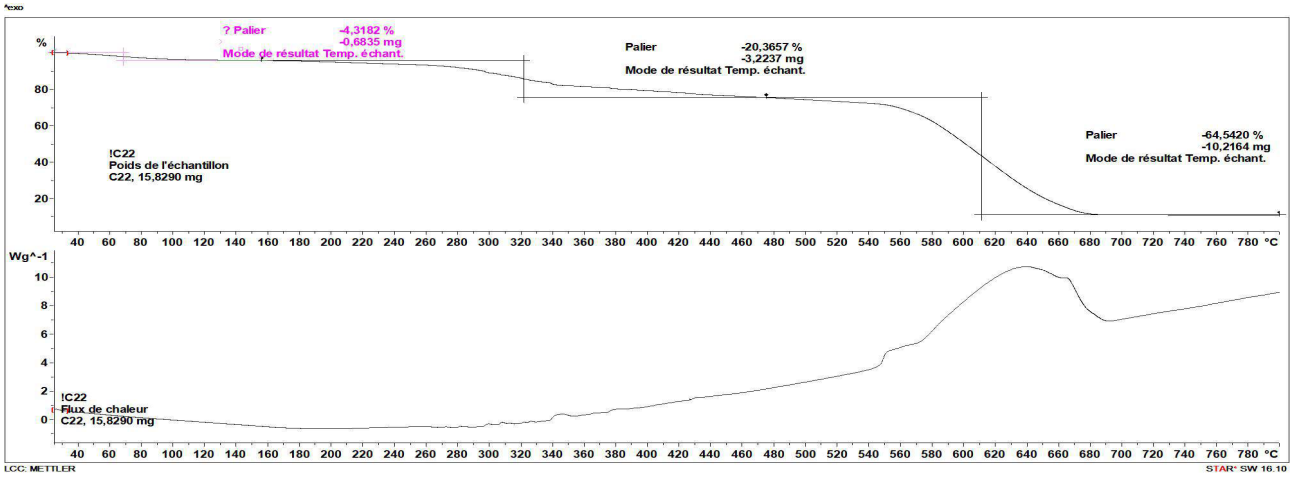

Figure S3. Thermograms of Zn(II) complexes.

Table S1. Value of Wiberg bond index (WBI) and of some properties of the electronic function at BCPs of coordination bonds in the studied complexes.

		L1Zn	L2Zn	L3Zn
Zn-N1	WBI	0.1116	0.1461	0.2062
	$\rho(r)$	0.0573	0.0447	0.0623
	$\nabla^2\rho(r)$	0.1995	0.1652	0.2122
	$H(r)$	−0.013973	−0.0057	−0.0177
	$-\frac{G(r)}{V(r)}$	0.8204	0.8589	0.7992
Zn-N4	WBI	0.1120	0.2330	0.1745
	$\rho(r)$	0.0432	0.0773	0.0391
	$\nabla^2\rho(r)$	0.1613	0.2435	0.1478
	$H(r)$	−0.0047	−0.0299	−0.0027
	$-\frac{G(r)}{V(r)}$	0.9016	0.7523	0.9354
Zn-N4'	WBI	0.1134	0.2341	0.1920
	$\rho(r)$	0.0535	0.0655	0.0512
	$\nabla^2\rho(r)$	0.1911	0.2158	0.1840
	$H(r)$	−0.0109	−0.0202	−0.0094
	$-\frac{G(r)}{V(r)}$	0.8429	0.7859	0.8548
Zn-Cl	WBI	0.4162	0.6555	0.6481
	$\rho(r)$	0.0797	0.0828	0.0803
	$\nabla^2\rho(r)$	0.1790	0.1828	0.1799
	$H(r)$	−0.0351	−0.0378	−0.0356
	$-\frac{G(r)}{V(r)}$	0.6946	0.6883	0.6935
Zn-Cl	WBI	0.4205	/	0.6423
	$\rho(r)$	0.0809	/	0.0801
	$\nabla^2\rho(r)$	0.1808	/	0.1793
	$H(r)$	−0.0361	/	−0.0353
	$-\frac{G(r)}{V(r)}$	0.7598	/	0.6941

Continued

Zn-O	WBI	/	0.2824	/
	$\rho(r)$		0.0723	
	$\nabla^2\rho(r)$		0.2749	
	$H(r)$		−0.0227	
	$-\frac{G(r)}{V(r)}$		0.8010	

Table S2. Values of selected parameters of the optimized geometry of ligands and Zn(II) complexes.

	L1	HL2	L3	L1Zn	L2Zn	L3Zn
Bond Length (Å)						
N1-C2	1.270	1.271	1.268	1.277	1.279	1.268
C2-C3	1.475	1.471	1.478	1.464	1.468	1.472
C3-N4	1.318	1.320	1.318	1.322	1.324	1.321
C3-C12	1.420	1.418	1.420	1.412	1.412	1.411
N4-C5	1.353	1.346	1.354	1.352	1.324	1.354
N1-C6’	1.391	1.391	1.450	1.395	1.374	1.440
C6’-C5’	1.432	1.432	1.507	1.428	1.435	1.509
C6’-C7’	1.384	1.384	/	1.381	1.382	/
C5’-N4’	1.356	1.356	1.336	1.353	1.365	1.333
N4’-C3’	1.313	1.313	1.334	1.313	1.318	1.335
C6-O	/	1.339	/	/	1.287	/
O-H	/	0.978	/	/	/	/
N1-Zn	/	/	/	2.197	2.316	2.160
N4-Zn	/	/	/	2.322	2.069	2.369
N4’-Zn	/	/	/	2.227	2.138	2.248
Cl-Zn	/	/	/	2.228	2.210	2.224
Cl’-Zn	/	/	/	2.221	/	2.225
O-Zn	/	/	/	/	2.052	/
Bond Angles (˚)						
Cl-Zn-N1	/	/	/	108.6	99.5	100.0
Cl-Zn-N4	/	/	/	93.4	117.7	98.1
Cl-Zn-N4’	/	/	/	97.7	99.8	102.4
Cl-Zn-Cl’(O)	/	/	/	128.9	114.2	129.4
N1-Zn-N4	/	/	/	72.8	70.3	72.3

Continued

N1-Zn-N4’	/	/	/	73.7	72.7	73.5
N1-Zn-Cl’(O)	/	/	/	122.5	142.4	130.6
N4-Zn-N4’	/	/	/	146.5	130.5	142.5
N4-Zn-Cl’(O)	/	/	/	100.2	79.2	96.5
N4’-Zn-Cl’(O)	/	/	/	97.1	114.9	94.3
Zn-N1-C2	/	/	/	116.8	115.0	119.9
Zn-N1-C6’	/	/	/	117.2	112.2	116.2
Zn-N4-C3	/	/	/	112.5	123.4	112.4
Zn-N4’-C5’	/	/	/	116.1	115.7	116.7
Dihedral Angles (˚)						
C6-C5-N4-C3	179.8	179.7	180.0	179.8	175.2	178.6
C5-N4-C3-C2	180.0	179.8	180.0	178.9	172.1	177.1
N4-C3-C2-N1	5.3	1.8	2.0	0.2	0.1	3.3
C3-C2-N1-C6’	175.0	175.5	178.0	179.7	172.0	173.6
C2-N1-C6’-C5’	129.7	131.2	105.9	167.7	164.0	159.7
N1-C6’-C5’-N4’	5.1	4.7	90.6	0.6	1.6	20.4
C6’-C5’-N4’-C3’	179.4	179.3	177.7	179.6	179.6	178.4

Table S3. Contact residues with compounds in the active sites of the proteins.

Compounds	SmCE2a	SER	SmTGR	SmPNP
L^3	**Chain A**: ARG21 VAL22 SER23 THR24 TRP25 ARG49 THR50 MET51 CYS52 HIS67 CYS68 SER71 TYR104 SER107 SER111 ILE117 GLN119 THR120 LEU121 ASP125 ARG166 ALA177 THR212 ALA213 PRO214 GLY215 SER217 VAL233 SER234 HIS235 GLY236	**Chain A**: TRP28 ILE29 THR60 HIS61 GLU89 ASP90 SER92 SER109 LYS111 VAL112 ARG114 GLU116 SER142 GLN147 ARG148 ASN149 GLU173 ASP174 ARG176 LYS177 GLN178 LEU235 ASP242 GLU264 CYS270 ARG271 ALA272 CYS273 LYS274 HIS275 ALA276 MET277 SER284 GLN285 CYS286 ASN308 HIS310 ASP311 ILE312 TYR327	**Chain A**: ILE113 GLY114 GLY115 GLY116 SER117 GLY118 GLY119 LEU136 ASP137 TYR138 VAL139 GLU140 TRP148 GLY152 THR153 CYS154 VAL157 GLY158 CYS159 LYS162 ALA226 LYS227 GLY228 ALA256 THR257 GLY258 GLU259 ARG260 SER276 PHE280 TYR296 VAL297 ALA390 VAL391 ARG393 GLN396 LYS399 VAL400 GLY432 ASP433 PRO439 GLN440 LEU441 THR442 PRO443 ALA445LEU484 SER485 ASP488 LYS492 HIS538 GLY545 GLU546 GLN549	**Chain A**: CYS33 GLY34 SER35 GLY36 LEU37 GLY85 ARG86 HIS88 TYR90 GLU91 ASN117 ALA118 ALA119 GLY120 TYR194 TYR202 GLU203 VAL219 GLY220 MET221 SER222 THR244 ASN245 HIS259 VAL262 LEU263 GLY266 ALA267 **Chain B**: ARG160 PHE161
HL^2	**Chain A**: VAL22 SER23 THR24 THR50 HIS67 SER71 PRO72 TYR104 SER107 ALA110 SER111 ARG112 ARG115 ARG116	**Chain A**: TRP28 HIS61 GLU89 ASP90 SER92 LYS111 VAL112 ARG114 GLU116 GLN147 ARG148 GLU173 ASP174	**Chain A**: ILE113 GLY114 GLY115 GLY116 SER117 GLY118 ASP137 TYR138 VAL139 GLU140 GLY152 THR153 CYS154 CYS159 LYS162 LYS227	**Chain A**: CYS33 GLY34 SER35 GLY36 LEU37 GLY38 GLY85 ARG86 HIS88 TYR90 GLU91 ASN117

	ILE117 GLN119 THR120 LEU121 SER122 ASP125 THR212 ALA213 PRO214 GLY215 SER217 VAL233 SER234 HIS235 GLY236	ARG266 GLY268 ASN269 CYS270 ARG271 ALA272 CYS273 LYS274 HIS275 ALA276 MET277 GLY280 LYS281 CYS282 VAL283 SER284 GLN285 CYS286 ASN308 HIS310 ASP311 ILE312 TYR327	ALA256 THR257 GLY258 GLU259 ARG260 GLY293 ALA294 SER295 TYR296 VAL297 LEU320 LEU321 ARG322 GLY323 PHE324 ASP325 ALA390 VAL391 GLY392 ARG393 GLN396 VAL400 GLY432 ASP433 GLY437 PRO439 GLN440 LEU441 THR442 PRO443 VAL444 ALA445 ILE446 ASP465 TYR466 SER467 ASN468 VAL469 ALA470 THR471 THR472 PHE474 TYR479 ALA481 CYS482 GLY483 LEU484 SER485 HIS538 GLY545 GLN549 ALA552 LYS556	ALA118 ALA119 GLY120 TYR194 TYR202 GLU203 VAL219 GLY220 MET221 SER222 THR244 ASN245 HIS259 VAL262 LEU263 ALA264 THR265 GLY266 ALA267 **Chain B**: ARG160 PHE161
2	**Chain A**: VAL22 SER23 THR24 THR50 MET51 CYS52 HIS67 CYS68 SER71 PRO72 TYR104 SER107 CYS108 ALA110 SER111 ARG112 ARG114 ARG115 ARG116 ILE117 GLN119 THR120 LEU121 SER122 ASP125 THR212 ALA213 PRO214 GLY215 SER217 SER234 HIS235 GLY236	**Chain A**: TRP28 ILE29 HIS61 GLU89 ASP90 SER92 LYS111 ARG114 GLU116 GLN147 ARG148 GLU264 GLY268 ASN269 CYS270 ARG271 ALA272 CYS273 LYS274 HIS275 ALA276 MET277 GLY280 SER284 GLN285 CYS286 ASN308 HIS310 ASP311 TYR327	**Chain A**: LYS262 GLY293 ALA294 SER295 TYR296 ARG317 SER318 ILE319 LEU321 ARG322 GLY323 PHE324 ALA390 VAL391 GLY392 ARG393 LYS438 PRO439 GLN440 LEU441 TYR466 SER467 ASN468 VAL469 THR471 GLY483 LEU484 SER485 ASP488	**Chain A**: CYS33 GLY34 SER35 GLY36 LEU37 GLY38 LYS39 GLN84 GLY85 ARG86 HIS88 TYR90 SER116 ASN117 ALA118 ALA119 GLY120 TYR202 GLU203 VAL219 GLY220 MET221 SER222 THR244 ASN245 HIS259 VAL262 LEU263 GLY266 ALA267 ALA270 **Chain B**: PHE161
Known Inhibitors	**Chain A**: VAL22 SER23 THR24 THR50 MET51 CYS52 HIS67 THR212 ALA213 PRO214 GLY215 ASP216 SER217 VAL233 SER234 HIS235 GLY236 **PMSF(**Phenylmethylsulfonyl Fluoride)	**Chain A**: TRP28 THR60 HIS61 GLU89 SER92 SER109 LYS111 ARG114 GLU116 PRO117 GLN147 ARG148 GLU264 ASN269 CYS270 ARG271 ALA272 CYS273 LYS274 HIS275 ALA276 MET277 ASP279 GLY280 LYS281 CYS282 SER284 GLN285 CYS286 ASN308 PHE309 HIS310 ASP311 ILE312 CYS313 TYR327 CYS328 VAL329 **Tyrphostin AG1478**	**Chain A**: GLU259 TYR296 VAL297 ARG322 GLY323 PHE324 ASP325 ARG393 ASP433 GLY437 LYS438 PRO439 GLN440 LEU441 PRO443 VAL444 ILE446 GLN447 ARG450 TYR451 GLU462 LEU463 THR464 ASP465 TYR466 SER467 ASN468 VAL469 ALA470 THR471 TYR479 ALA481 CYS482 GLY483 LEU484 SER485 ASP488 HIS538 GLN549 ALA552 VAL553 LYS556 **AURANOFIN**	CYS33 GLY34 SER35 GLY36 LEU37 THR61 GLN84 GLY85 ARG86 HIS88 TYR90 SER116 ASN117 ALA118 ALA119 GLY120 TYR194 TYR202 GLU203 VAL219 GLY220 MET221 SER222 THR244 ASN245 HIS259 VAL262 LEU263 THR265 GLY266 ALA267 **Chain B**: PHE161 **NEOLIGNAN**